Radiology

Imaging of Pulmonary Vasculitis[1]

Man Pyo Chung, MD
Chin A Yi, MD
Ho Yun Lee, MD
Joungho Han, MD
Kyung Soo Lee, MD

The presence of pulmonary vasculitis can be suggested by a clinical presentation that includes diffuse pulmonary hemorrhage, acute glomerulonephritis, chronic refractory sinusitis or rhinorrhea, imaging findings of nodules or cavities, mononeuritis multiplex, multisystemic disease, and palpable purpura. Serologic tests, including the use of cytoplasmic antineutrophil cytoplasmic antibody (ANCA) and perinuclear ANCA, are performed for the differential diagnosis of the diseases. A positive cytoplasmic ANCA test result is specific enough to make a diagnosis of ANCA-associated granulomatous vasculitis if the clinical features are typical. Perinuclear ANCA positivity raises the possibility of Churg-Strauss syndrome or microscopic polyangiitis. Imaging findings of pulmonary vasculitis are diverse and often poorly specific. The use of a pattern-based approach to the imaging findings may help narrow the differential diagnosis of various pulmonary vasculitides. Integration of clinical, laboratory, and imaging findings is mandatory for making a reasonably specific diagnosis.

[1]From the Division of Pulmonary and Critical Care Medicine, Department of Internal Medicine (M.P.C.), Department of Radiology and Center for Imaging Science (C.A.Y., H.Y.L., K.S.L.), and Department of Pathology (J.H.), Samsung Medical Center, Sungkyunkwan University School of Medicine, 50 Ilwon-Dong, Kangnam-Ku, Seoul 135-710, Korea. Received January 16, 2009; revision requested March 24; revision received April 9; accepted May 8; final version accepted June 1; final review by K.S.L. December 10. **Address correspondence to** K.S.L. (e-mail: *kyungs.lee@samsung.com*).

Pulmonary vasculitides are noninfectious inflammatory disorders that mainly affect the blood vessels of the lung, from the main pulmonary artery to alveolar capillaries (1,2). Histopathologically, they refer to a condition where acute or chronic cellular inflammation occurs within vessel walls and subsequently leads to blood vessel destruction and surrounding lung tissue necrosis (1). The pulmonary vasculitides encompass a clinically, radiologically, and histopathologically heterogeneous group of diseases and are usually associated with systemic vasculitis (1,2).

Since pulmonary vasculitides include various diseases, specific imaging findings cannot be expected. However, several clinical symptoms and signs are suggestive of the presence of pulmonary vasculitis (1,3), and laboratory study results are helpful to reach a specific diagnosis or, at least, to narrow the differential diagnosis to a distinct entity (4–9).

Imaging findings of pulmonary vasculitis are variable and poorly specific (10–14). As isolated findings or as combined findings, diffuse ground-glass opacity (GGO) (associated with diffuse alveolar hemorrhage [DAH]), focal or patchy areas of GGO or consolidation, cavitating and noncavitating nodules, poorly defined centrilobular small nodules (nodules <10 mm in diameter), and vascular tree-in-bud signs (small centrilobular nodules and nodular branching structures) (10) can be observed. During the past decade, several review articles about imaging findings of pulmonary vasculitis have been published (11–14). However, a detailed review of the literature on the imaging findings of pulmonary vasculitis and suggestions for an algorithmic approach to pulmonary vasculitis based on imaging and clinical findings are not available.

The purposes of this review were to classify the various types of pulmonary vasculitis according to the modified Chapel Hill consensus classification (15), to describe clinical manifestations of each disease entity, to propose diagnostic criteria for the diseases, to present key important imaging findings, and to compare imaging findings with findings of pathologic examination.

Essentials

- When pulmonary vasculitis is being considered, a pattern approach based on radiologic findings may help to refine or narrow the differential diagnosis.
- Integration of clinical, laboratory, and imaging findings is mandatory for making a specific diagnosis of various pulmonary vasculitides.

Etiology and Pathogenesis

Pulmonary vasculitis is associated with granulomatous, eosinophilic, lymphoplasmocytic, or neutrophilic inflammatory diseases (1) and commonly is a manifestation of systemic illnesses such as primary systemic vasculitides, collagen vascular diseases, systemic diseases associated with the autoantibodies, and as a side effect of certain drugs such as propylthiouracil and diphenylhydantoin (1). However, pulmonary vasculitis can occur in isolation without the involvement of other organs (16).

Although the inciting antigens or stimuli of vasculitis are not well understood, an immunologic mechanism is involved in the pathogenesis of antineutrophil cytoplasmic antibody (ANCA)-associated vasculitis (17). ANCA has two major staining patterns: cytoplasmic and perinuclear. In ANCA-associated vasculitis, an intense infiltration of activated neutrophils results in fibrinoid necrosis and dissolution of vessel walls, thus compromising the vascular lumen. ANCA may be involved in the pathogenesis not only by activation of neutrophils but also by enhancement of the adhesion of the activated neutrophils to cytokine-primed endothelial cells. The damage to the integrity of the vessels results in the leakage of blood into the alveolar space from the interstitial capillaries and causes stenoses, thrombotic obstruction, and aneurysms of the corresponding vessels (9,17). Clinically, the damage is manifested as DAH and on imaging studies, as lung nodules, consolidation, GGOs, pulmonary thromboembolism, pulmonary artery aneurysm, or stenosis of the pulmonary artery. Repeated episodes of DAH can lead to progressive lung fibrosis (18).

The production of autoantibodies such as antiglomerular basement membrane antibody (type 2 hypersensitivity reaction), formation of immune complexes (type 3 hypersensitivity reaction), and T cell involvement (type 4 hypersensitivity reaction) are likely to link to the pathogenesis of other forms of small-vessel pulmonary vasculitis. This process may be collectively called immune complex–mediated vasculitis (1,15). Vasculitis in systemic lupus erythematosus (SLE) is typical of this immune complex–mediated vascular disease (1,3,15,19).

Classification

The Chapel Hill consensus conference held in 1992 to determine a consistent nomenclature and a definition of noninfectious systemic vasculitis for the entire body has provided a basic framework for the disease (15). The Chapel Hill classification is based on both the size of the vessels involved and the laboratory findings (15). Giant cell arteritis, polyarteritis nodosa, and Kawasaki disease are initially included in the Chapel Hill consensus classification. However, in these three diseases, pulmonary vessels are rarely involved (1,15). Therefore, we do not discuss these three diseases in this review nor do we include these diseases in Figure 1. The vasculitides that are not included in the Chapel Hill consensus classification but involve pulmonary vasculature comprise isolated pauci-immune pulmonary capillaritis, vasculitis associated with collagen vascular diseases that include

Published online
10.1148/radiol.10090105

Radiology 2010; 255:322–341

Abbreviations:
ANCA = antineutrophil cytoplasmic antibody
CSS = Churg-Strauss syndrome
DAH = diffuse alveolar hemorrhage
GGO = ground-glass opacity
Ig = immunoglobulin
SLE = systemic lupus erythematosus

Authors stated no financial relationship to disclose.

Figure 1

Included in the Chapel Hill Nomenclature	Not Included in the Chapel Hill Nomenclature
Large-vessel vasculitis	Isolated pauci-immune pulmonary capillaritis
Takayasu arteritis	Behçet disease
Small-vessel vasculitis	Hughes-Stovin syndrome
ANCA-associated vasculitis	Vasculitis associated with collagen vascular diseases
Wegener granulomatosis	SLE
Churg-Strauss syndrome (CSS)	Rheumatoid arthritis
Microscopic polyangiitis	Primary antiphospholipid syndrome, etc
Henoch-Schonlein purpura	Drug- and foreign material–induced vasculitis
Essential cryoglobulinemic vasculitis	Drugs: propylthiouracil, gemcitabine, diphenylhydantoin, ransretinoic acid, crack cocaine
Cutaneous leukocytoclastic angiitis	Foreign materials: talc, starch, cellulose, maltose
	Goodpasture syndrome
	IgA nephropathy
	Others

Figure 1: Modified Chapel Hill classification of pulmonary vasculitis.

Behçet disease, SLE, drug-induced vasculitis, Goodpasture syndrome, immunoglobulin (Ig) A nephropathy, and Hughes-Stovin syndrome (Fig 1). We will discuss these diseases in addition to the ones included in the original Chapel Hill classification. The Chapel Hill classification is still valid because it is a useful framework that classifies pulmonary vasculitis according to vessel size, thus helps explain clinical-pathologic features. However, the classification needs revision because it does not consider the pathogenetic mechanism of various vasculitides (1).

According to their vessel size and internal components, pulmonary vessels can be classified into four categories: *(a)* elastic arteries (≥1 mm in the external diameter and containing numerous elastic laminae), *(b)* muscular arteries (<1 mm but >100 μm in diameter and containing a thin smooth-muscle media layer bounded by internal and external elastic lamina), *(c)* arterioles (<100 μm in diameter and consisting of a layer of endothelial cells on an elastic lamina), and *(d)* capillaries (<10 μm in diameter and consisting of a layer of endothelial cells and basement membrane) (2).

In the Chapel Hill classification, "large artery" refers to the aorta and the largest branches directed toward major body regions, "medium-sized artery" refers to the main visceral arteries, and "small artery" refers to the distal intraparenchymal arterial tributaries connected to arterioles. In pulmonary vasculitis of Takayasu arteritis, Behçet disease, and Hughes-Stovin syndrome, elastic pulmonary arteries, hence large- or medium-sized vessels according to the Chapel Hill classification, are involved. In the remaining pulmonary vasculitides, muscular arteries, arterioles, or capillaries may be involved, thus may be collectively called small-vessel disease according to the Chapel Hill classification. Pulmonary capillaries and venules are exclusively involved in cutaneous leukocytoclastic angiitis and Goodpasture syndrome (1–3,15).

Since ANCAs are frequently present in ANCA-associated granulomatous vasculitis, CSS and microscopic polyangiitis, these diseases are collectively called ANCA-associated vasculitis (4–9,15). Goodpasture syndrome can be classified as antiglomerular basement membrane antibody vasculitis, because the syndrome is caused by the autoimmune antibody (antiglomerular basement membrane antibody) attacking the Goodpasture antigen, which is found in the kidneys and lungs (15). Other small-vessel pulmonary vasculitides such as in SLE, where immune complex formation and T cell involvement are the pathogenic mechanism, may be classified as immune complex–mediated small-vessel pulmonary vasculitis.

Clinical Findings That Suggest Pulmonary Vasculitis

A suspicion of pulmonary vasculitis starts with the clinical presentation of the patient (1,3). Most commonly, patients with pulmonary vasculitis present with various multisystem manifestations (1,3). Although combined manifestations are more common, each of the following symptoms and signs can be seen as an isolated symptom or a sign: diffuse pulmonary hemorrhage, glomerulonephritis, upper respiratory tract lesions, imaging findings of nodules or cavitary lesions, mononeuritis multiplex, multisystem disease, and palpable purpura (1,3).

Laboratory Tests

ANCAs, detected by using an indirect immunofluorescence test with ethanol-fixed neutrophils as a substrate, are autoantibodies that act against various antigens present in the cytoplasmic granules of neutrophils and lysosomes of monocytes (6–9). ANCA tests play an important role in the diagnosis of some pulmonary vasculitides, including ANCA-associated granulomatous vasculitis, CSS, and microscopic polyangiitis, and for idiopathic pauci-immune rapidly progressive glomerulonephritis. The diseases have common clinical features, pathologic involvement of the small vessels, similar responses to immunosuppressive treatment, and ANCA positivity (1).

Cytoplasmic ANCA, perinuclear ANCA, and atypical ANCA are described according to the results of indirect immunofluorescent staining patterns. Cytoplasmic ANCA is mainly related to antibodies directed against proteinase 3 found in azurophilic granules of neutrophils and monocytes, whereas perinuclear ANCA is associated with antibodies directed against a variety of intracellular antigens (most commonly with myeloperoxidase, also found in azurophilic granules) (4–9).

The use of cytoplasmic ANCA is highly sensitive (90%–95%) for the detection of active, systemic ANCA-associated granulomatous vasculitis and has a specificity of approximately 90% (4). In an adequate clinical setting, a positive cytoplasmic ANCA finding has sufficient positive predictive value (>90%) so that a biopsy may be deferred or exempted (1,3). Conversely, a positive perinuclear ANCA finding provides no more than suggestive evidence of CSS,

Figure 2

a.

b.

c.

Figure 2: **(a)** Chest radiograph in a 30-year-old man with Takayasu arteritis shows enlarged heart and enlarged bilateral pulmonary arteries. Note oligemic left upper lung zone (arrows). **(b)** Contrast-enhanced transverse CT scan in the same patient shows marked wall thickening and luminal narrowing in proximal left pulmonary artery (arrows). Note wall thickening (arrowheads) in ascending and descending thoracic aorta. Left pleural effusion is associated. **(c)** Coronal PET scan in another patient with Takayasu arteritis shows increased fluorodeoxyglucose uptake in main pulmonary artery (arrow) and ascending aorta (arrowhead), suggesting active inflammatory stage of disease.

microscopic polyangiitis, or idiopathic pauci-immune rapidly progressive glomerulonephritis (4,5). Perinuclear ANCA can be found in diseases such as rheumatoid arthritis, Goodpasture syndrome, infection (hepatitis C, fungal, and mycobacterial), and inflammatory bowel disease (6,7,20,21). When cytoplasmic or perinuclear ANCA finding is positive, the addition of proteinase 3 or myeloperoxidase ANCA enzyme-linked immunosorbent assay test can help increase the specificity in the diagnosis of ANCA-associated vasculitis (1).

The importance of increasing ANCA titers to predict relapse in patients with vasculitides has also been evaluated. Current studies suggest that there is insufficient sensitivity and specificity of an isolated increase in the ANCA titer to accurately predict relapse in ANCA-associated granulomatous vasculitis and other vasculitides (8,9).

Takayasu Arteritis

Takayasu arteritis is an idiopathic chronic arteritis resulting in the stenosis of a large-sized artery with a strong predilection for the aortic arch and its branches. The estimated annual incidence of Takayasu arteritis is 0.12–0.26 case per 100 000 (22). Pulmonary artery involvement occurs in 15% of patients (23).

Clinical and Histologic Findings

The disease is characterized by the presence of patchy panarteritis and is divided into acute inflammatory and healed fibrotic phases. In the acute inflammatory phase, the adventitia shows vasculitis in the vasa vasorum, the media demonstrates lymphocytic infiltration, and the intima shows thickening with mucopolysaccharides, smooth muscle cells, and fibroblasts (24,25). In the healed fibrotic phase, the fibrosis is accompanied by elastic tissue destruction

F igure 3

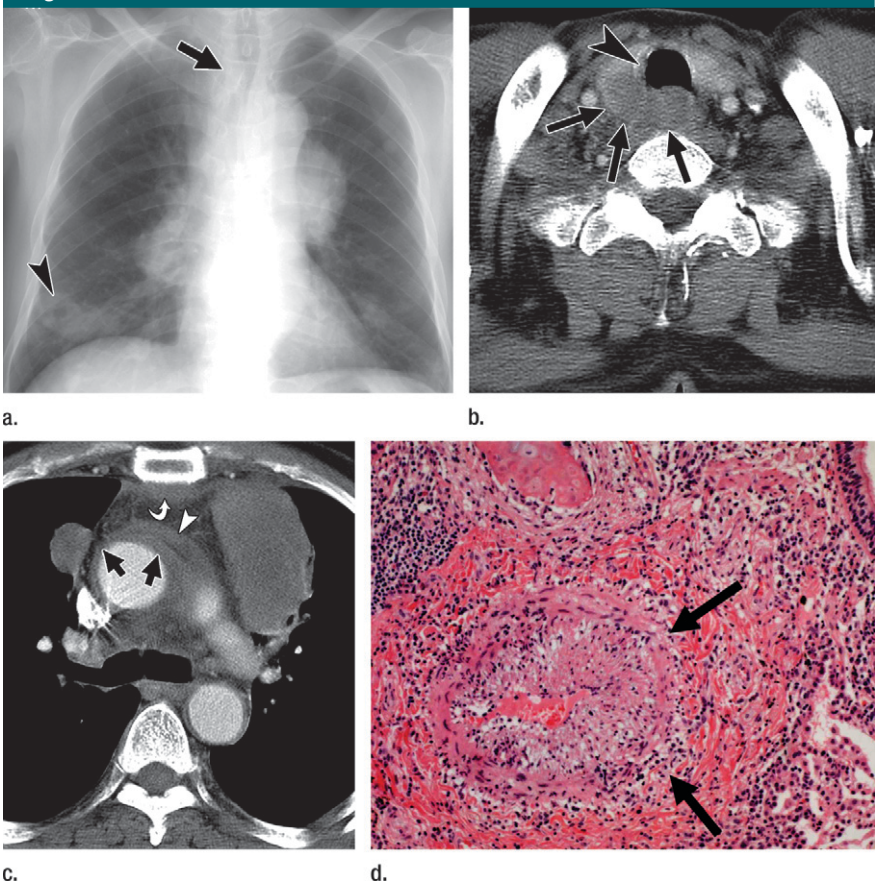

Figure 3: ANCA-associated granulomatous vasculitis in 57-year-old man. **(a)** Chest radiograph shows multiple variable-sized masses and nodules in both lungs. Nodule in right lower lung zone has internal cavitation (arrowhead). Note focal eccentric narrowing (arrow) of tracheal air column at thoracic inlet. **(b)** Contrast-enhanced CT scan shows low-attenuation soft-tissue mass lesion (arrows), posterolateral to right side trachea. Lesion has invaded into right thyroid gland. Note mild eccentric wall thickening of trachea (arrowhead), anterior to mass lesion. **(c)** CT scan at carinal level shows mass in left upper lobe and nodule in right upper lobe. Note thickening of ascending aortic wall (black arrows) and pericardium (arrowhead), probably associated with this vasculitis. Retrosternal bandlike structure (white arrow) is presumed to be caused by secondary fibrosing mediastinitis. **(d)** Bronchoscopic biopsy specimen from tracheal wall discloses chronic inflammatory cell infiltration with fibrosis in submucosal area. Note vascular luminal narrowing due to marked fibrotic medial thickening (arrows). (Hematoxylin-eosin stain; original magnification, ×100.)

and narrowing or obliteration of the arterial lumen (24,25).

Pulmonary involvement usually occurs in patients who have systemic vasculitis. However, there is no correlation between systemic arteritis and the extent of pulmonary arterial involvement (26). Rarely, it may be the first manifestation of the disease. When a pulmonary artery is substantially narrowed, atypical chest pain and dyspnea may develop. Generalized symptoms that include malaise, fever, night sweating, arthralgia, anorexia, and weight loss may occur before vascular involvement is apparent. Commonly, a radial pulse is absent in patients with subclavian artery occlusion (27).

Imaging Findings

Chest radiographic findings of Takayasu arteritis, which represent healed fibrotic phase of the disease, include, in decreasing order of frequency, irregular contour of the descending aorta, linear calcification of the aortic wall, ectatic aortic arch, cardiomegaly, and decreased pulmonary vascular markings (26) (Fig 2).

Computed tomographic (CT) scans without contrast material show a high-attenuation aortic or pulmonary artery wall with or without calcification. Increased attenuation in mediastinal fat may be seen in the surrounding areas of the aorta and main pulmonary artery as a sign of active inflammation (28). On early arterial-phase contrast material–enhanced images, circumferential wall thickening of 1–4 mm is observed (Fig 2). Delayed enhancement of a thickened aortic or pulmonary arterial wall, as depicted on scans obtained 20–40 minutes after contrast medium injection, is characteristic of the active inflammatory phase of the disease (28). The most common findings of pulmonary arterial involvement include stenosis or occlusion of segmental or subsegmental arteries, usually in the upper lobes. The vascular abnormalities may accompany areas of mosaic perfusion in the corresponding lung parenchyma (28) (Fig 2). Delayed enhancement, which is observed at CT in the actively inflamed arterial wall, has also been shown at magnetic resonance (MR) imaging (29). Contrast-enhanced MR imaging provides information about disease activity of Takayasu arteritis; more enhancement of thickened aortic wall as compared with that of the myocardium suggests active disease and is consistent with laboratory findings suggesting active inflammation (30). The use of fluorine 18 fluorodeoxyglucose positron emission tomography (PET) demonstrates increased fluorodeoxyglucose uptake in the involved arteries, also indicating active inflammatory disease (31) (Fig 2).

In the healed fibrotic phase, CT scans show calcified vascular walls. The calcification more commonly involves the entire wall, reflecting the transmural nature of the inflammation. In the fibrotic phase, the arterial wall does not enhance after administration of contrast material (28).

Differential Diagnosis

Takayasu arteritis should be differentiated from arteriosclerosis, thromboangiitis

F-igure 4

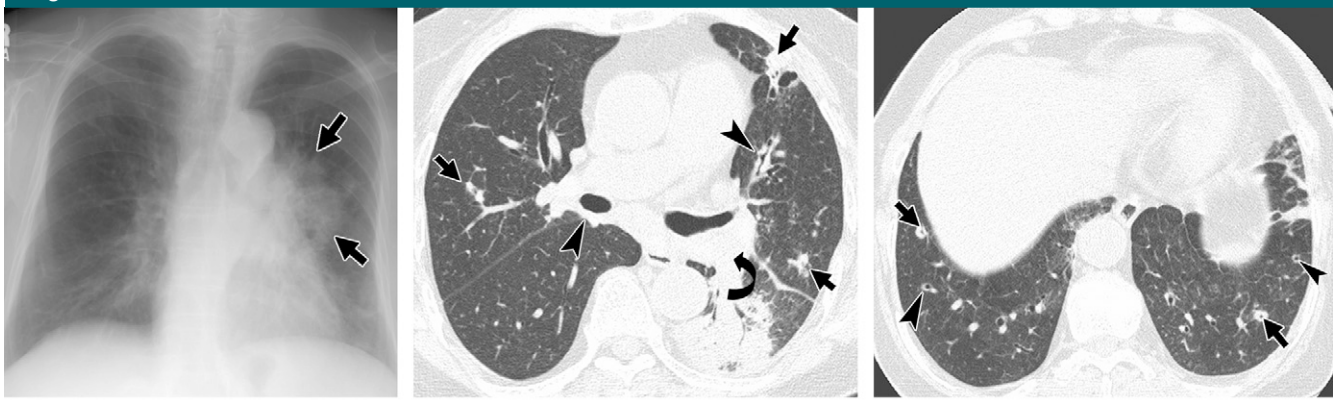

a. b. c.

Figure 4: ANCA-associated granulomatous vasculitis in 78-year-old woman. **(a)** Chest radiograph shows masslike consolidation (arrows) in left parahilar area and increased interstitial lung markings in right lung and left lower lung zone. **(b)** Thin-section CT scan at level of bronchus intermedius shows consolidation in superior segment of left lower lobe and variable-sized nodular lesions (straight arrows) in both lungs. Note bronchial wall thickening (arrowheads) in posterior wall of bronchus intermedius and anterior segmental bronchus of left upper lobe and obliteration (curved arrow) of arising portion of lower lobar and superior segmental bronchus of left lower lobe. **(c)** CT scan at level of liver dome shows cavitating nodules (arrows) and bronchial wall thickening (arrowheads) in both lower lobes.

Figure 5

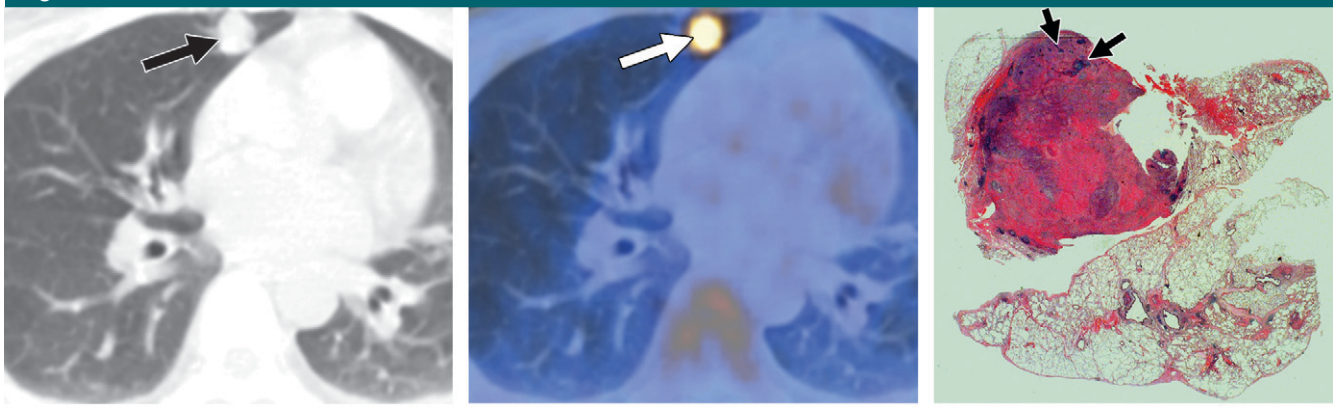

a. b. c.

Figure 5: ANCA-associated granulomatous vasculitis manifesting as solitary pulmonary nodule in 51-year-old woman. **(a)** Lung window of transverse CT scan obtained at level of basal trunk shows 13-mm nodule (arrow) in right middle lobe. **(b)** PET/CT image shows high (peak standardized uptake value, 5.4) fluorodeoxyglucose uptake (arrow) in the nodule. **(c)** Low-magnification pathologic specimen obtained by using video-assisted thoracoscopic biopsy shows basophilic inflammatory nodule containing geographic necrotic areas (arrows). (Hematoxylin-eosin stain; original magnification, ×40.)

obliterans (Buerger disease), and syphilitic aortitis. Aortic wall thickening with high attenuation on unenhanced scans and delayed enhancement in acute inflammatory phase, transmural wall calcification, and absence of enhancement in healed fibrotic phase are the key findings. In Buerger disease, peripheral arteries are narrowed. Calcifications in Takayasu arteritis are linear in shape and affect both the aortic arch and the descending aorta, as opposed to syphilic aortitis, in which calcification of the ascending aorta predominates (26,32,33).

ANCA-associated Granulomatous Vasculitis

ANCA-associated granulomatous vasculitis (previously carrying the now abandoned eponym Wegener granulomatosis [(34]) is characterized by necrotizing granulomatous inflammation with the classic triad of upper airway involvement (sinusitis, otitis, ulcerations, bone deformities, subglottic or bronchial stenosis) (Fig 3), lower respiratory tract involvement (cough, chest pain, dyspnea, and hemoptysis) (Figs 4, 5), and glomerulonephritis (hematuria, red blood cell casts, proteinuria, and azotemia). The median age of onset is 45 years (35). The annual incidence of ANCA-associated granulomatous vasculitis is estimated to be one case per 100 000 (36).

Figure 6

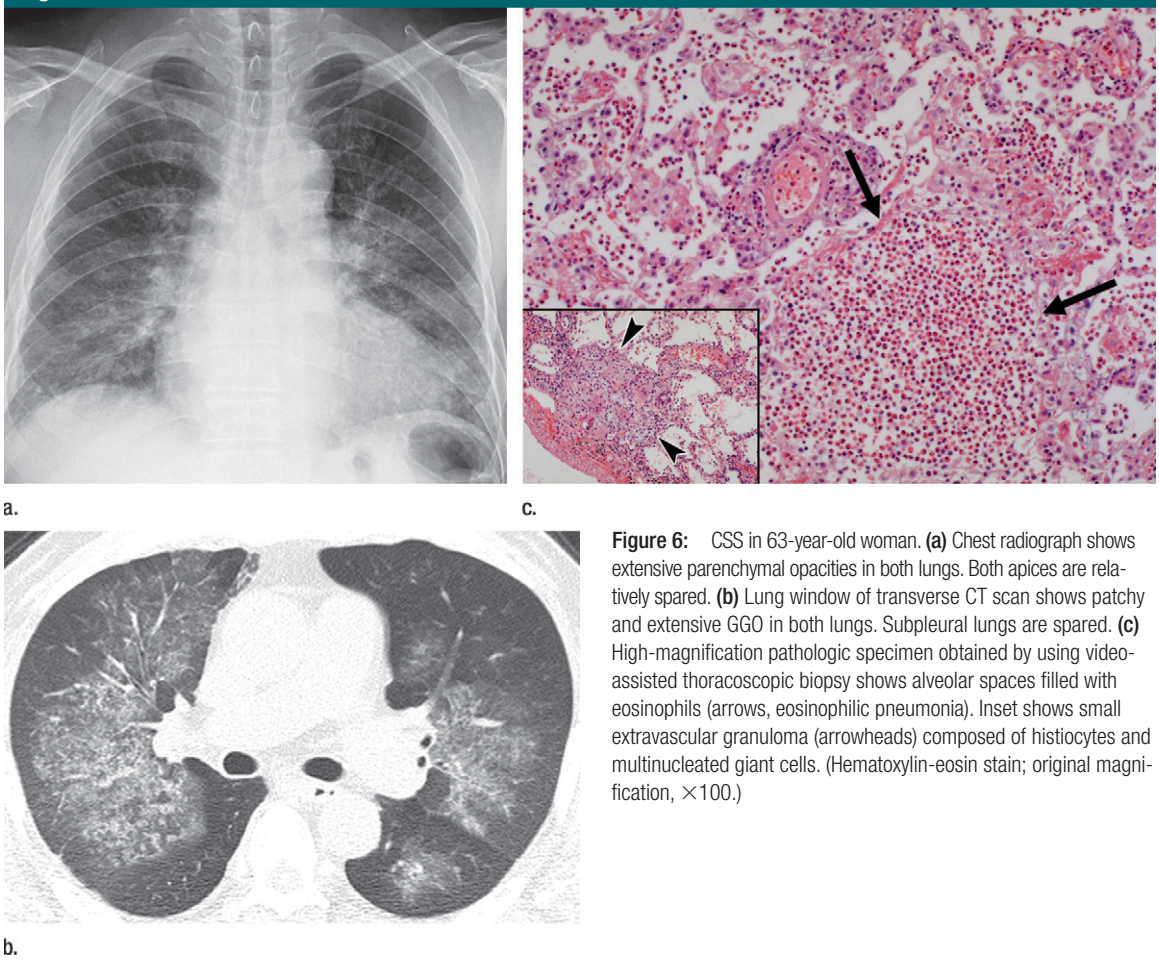

Figure 6: CSS in 63-year-old woman. **(a)** Chest radiograph shows extensive parenchymal opacities in both lungs. Both apices are relatively spared. **(b)** Lung window of transverse CT scan shows patchy and extensive GGO in both lungs. Subpleural lungs are spared. **(c)** High-magnification pathologic specimen obtained by using video-assisted thoracoscopic biopsy shows alveolar spaces filled with eosinophils (arrows, eosinophilic pneumonia). Inset shows small extravascular granuloma (arrowheads) composed of histiocytes and multinucleated giant cells. (Hematoxylin-eosin stain; original magnification, ×100.)

Clinical and Histologic Findings

The classic histologic pattern of pulmonary involvement of ANCA-associated granulomatous vasculitis is characterized by the presence of multiple bilateral pulmonary nodules with frequent cavitation that are composed of large areas of parenchymal necrosis, granulomatous inflammation, and vasculitis (Figs 3, 5) (37). Parenchymal necrosis can take the form of either neutrophilic microabscesses or a large zone of geographic necrosis that usually appears deeply basophilic due to the presence of nuclear debris of neutrophils (Fig 5). The surrounding inflammatory infiltrate consists of a mixture of neutrophils, lymphocytes, plasma cells, macrophages, giant cells, and eosinophils (37). Coexisting areas of granulomatous inflammation are also common and are characterized by the presence of palisading histiocytes that are arranged with their long axes perpendicular to the necrotic center. The vasculitis of ANCA-associated granulomatous vasculitis may affect arteries, veins, or capillaries, where vessel walls are partly or completely replaced by inflammatory infiltrates that contain varying proportions of neutrophils, lymphocytes, eosinophils, and epithelioid histiocytes. Necrotizing granulomas or cicatricial vascular changes may also be seen (37). In addition to the cases of the classic histologic pattern, those of several histologic variants, including a bronchocentric variant (38), eosinophilic variant (39), cryptogenic organizing pneumonia-like variant (40), and capillaritis variant (41), have been recognized.

Constitutional symptoms that include fever, arthralgia, myalgia, and weight loss and ocular involvement are common. Massive pulmonary hemorrhage is a life-threatening manifestation of ANCA-associated granulomatous vasculitis and requires aggressive immunosuppressive therapy as soon as possible. DAH is suspected when diffuse alveolar opacities as seen on a chest radiograph and a sudden decrease in the peripheral blood hematocrit level occur simultaneously with or without hemoptysis. As compared with the generalized form of ANCA-associated granulomatous vasculitis, as few as 40% of patients have renal involvement at the initial presentation (limited ANCA-associated granulomatous vasculitis). However, 80%–90% of patients are known to develop

Figure 7

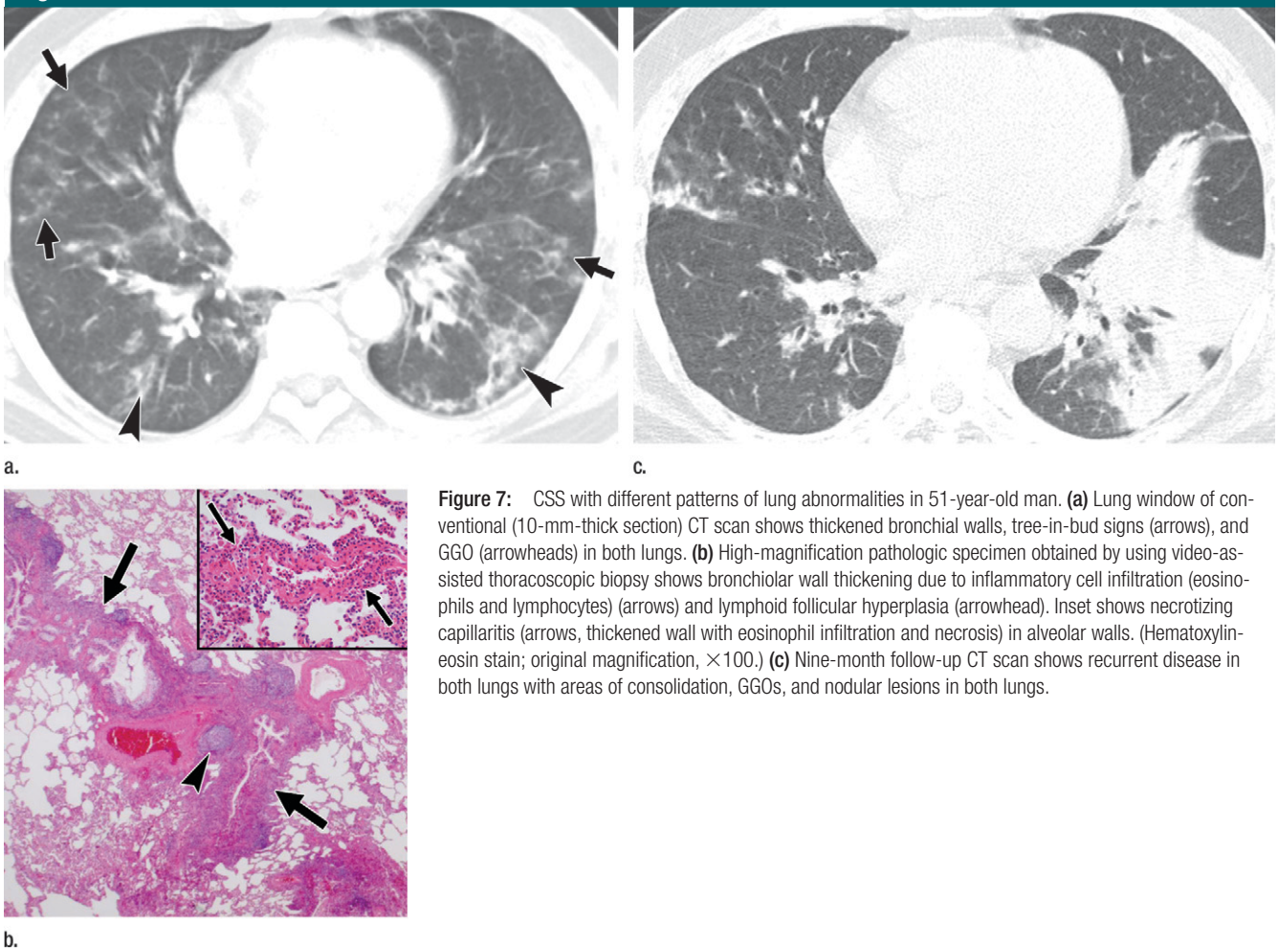

Figure 7: CSS with different patterns of lung abnormalities in 51-year-old man. **(a)** Lung window of conventional (10-mm-thick section) CT scan shows thickened bronchial walls, tree-in-bud signs (arrows), and GGO (arrowheads) in both lungs. **(b)** High-magnification pathologic specimen obtained by using video-assisted thoracoscopic biopsy shows bronchiolar wall thickening due to inflammatory cell infiltration (eosinophils and lymphocytes) (arrows) and lymphoid follicular hyperplasia (arrowhead). Inset shows necrotizing capillaritis (arrows, thickened wall with eosinophil infiltration and necrosis) in alveolar walls. (Hematoxylin-eosin stain; original magnification, ×100.) **(c)** Nine-month follow-up CT scan shows recurrent disease in both lungs with areas of consolidation, GGOs, and nodular lesions in both lungs.

renal disease. Cytoplasmic ANCA is positive in more than 90% of patients with the generalized form of ANCA-associated granulomatous vasculitis, but it is detected in half of patients with the limited form of the disease (4). Diagnosis of ANCA-associated granulomatous vasculitis can be confirmed when vasculitis is present on a biopsy specimen or at angiography plus when at least two of the following criteria are met: *(a)* nasal discharge (purulent or bloody) or oral ulcers, *(b)* abnormal urinary sediment (red cell casts or >5 red blood cells per high-power field), *(c)* abnormal findings on a chest radiograph (nodules, cavities, or fixed infiltrates), or *(d)* granulomatous inflammation within the artery wall or in the perivascular or extravascular area (presence of hemoptysis if biopsy is not available) (42). Sensitivity and specificity of these diagnostic criteria are reported to be 88% and 92%, respectively (42).

With the introduction of the use of cyclophosphamide in immunosuppressive therapy, complete remission has been achieved in 70%–90% of patients, but relapses are common. A poor prognosis is associated with DAH, severe azotemia, an advanced age, and positivity for proteinase 3 ANCA (35).

Imaging Findings

The most common radiographic abnormality is pulmonary nodules or consolidation with cavitation (43,44) (Figs 3, 4). Less frequent radiographic findings consist of nodule (s) without cavitation, increased bronchovascular lines involving the lung parenchyma (Fig 4), mediastinal or hilar lymph node enlargement, and pleural effusion (43,45). When radiographic findings are correlated with disease activity, nodules or masses and areas of parenchymal opacification are associated with active inflammatory lesions and show response to cyclophosphamide and corticosteroid treatment (46).

According to one study (47), the most common pattern on CT images at the initial presentation is the presence of nodules or masses in 90% (27 of 30) of patients (Figs 3–5). The nodules or masses are multiple in 85% of patients, bilateral in 67% of patients, subpleural

Figure 8

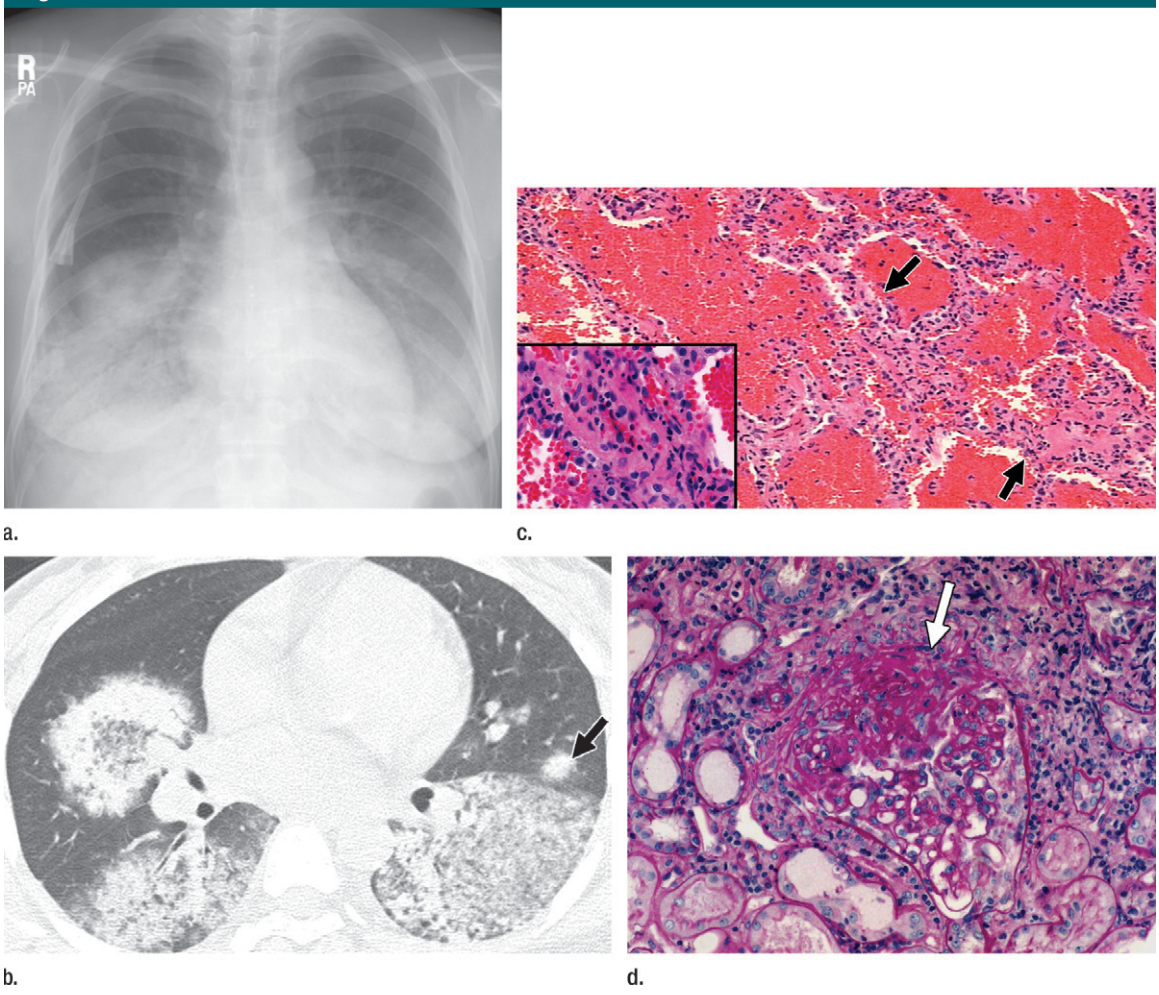

Figure 8: Microscopic polyangiitis in 33-year-old woman. **(a)** Chest radiograph shows extensive consolidation in bilateral middle and lower lung zones. Central venous line is inserted. **(b)** Lung window of CT scan shows extensive parenchymal opacities in both lungs. Poorly defined nodule (arrow) is observed in left upper lobe. **(c)** High-magnification pathologic specimen obtained by using video-assisted thoracoscopic biopsy shows intra-alveolar hemorrhage and thickened alveolar walls with neutrophilic infiltration (arrows). Inset shows neutrophilic capillaritis as focus of inflammation and karyorrhexis. (Hematoxylin-eosin stain; original magnification, ×100.) **(d)** High-magnification kidney biopsy specimen shows segmental necrotizing glomerulonephritis (arrow). (Periodic Acid Schiff stain; original magnification, ×200.)

in 89% of patients, and peribronchovascular in 41% of patients based on the distribution seen on CT images. Bronchial wall thickening in the segmental or subsegmental bronchi is seen in approximately 70% of patients (Fig 4). Large airways are also abnormal in 30% of patients (Fig 3). The subglottic trachea is the predilection site and its involvement may eventually lead to subglottic stenosis to such a degree that it necessitates tracheostomy (43). Another common manifestation is air-space consolidation and GGO, seen in 25%–50% of cases (44,47,48). These opacities are random or patchy in distribution (48) and are regarded to represent DAH caused by necrotizing capillaritis (47,48) (Please refer to DAH findings in microscopic polyangiitis.) Centrilobular nodules and a tree-in-bud sign pattern may be seen in up to 10% of patients, usually mixed with other changes such as nodules, masses, GGO, and bronchial wall thickening (47). These centrilobular small nodules and the tree-in-bud sign may result from bronchiolar inflammatory changes rather than from vasculitis (47).

Follow-up CT examination findings obtained after treatment show a decrease in the extent of the abnormalities in almost all cases. Lesions disappear completely, without scarring, in about half of the patients with pulmonary nodules or consolidation. Only a small proportion of patients have residual scarring. All GGO lesions also disappear. Masses show a decrease in the extent with residual scarring (44,49–51). If present, airway lesions show improvement with treatment in most patients (47).

Figure 9

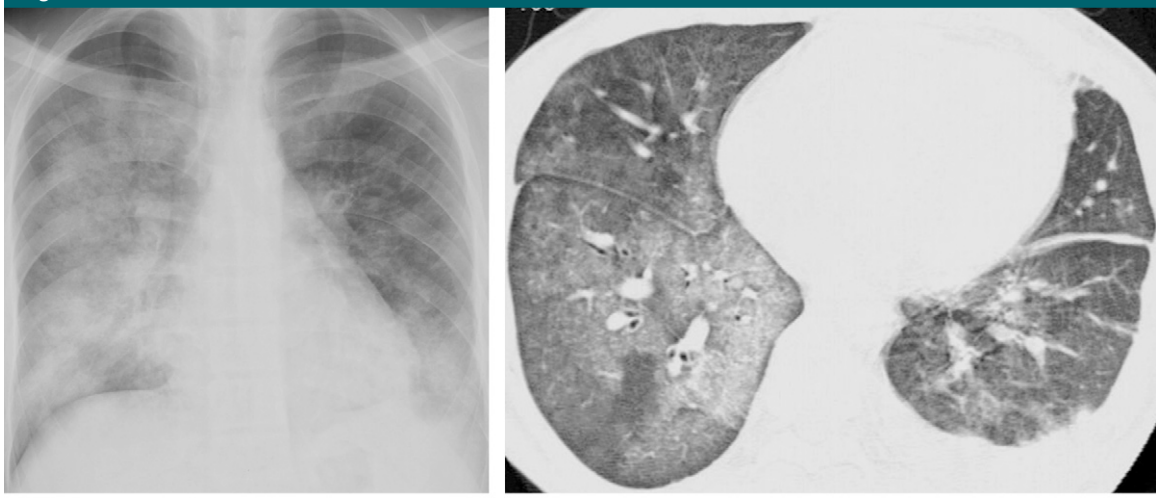

a. b.

Figure 9: Henoch-Schonlein purpura-associated pulmonary vasculitis in 25-year-old man complaining of hemoptysis, dyspnea, melena, and purpura. **(a)** Chest radiograph shows extensive parenchymal opacity in both lungs. Right lung is more extensively involved than left lung. Note apical sparing of lung lesions. **(b)** Lung window of CT scan shows extensive parenchymal opacity in both lungs. Note left pleural and fissural effusions. (Images courtesy of Joon Beom Seo, MD.)

Differential Diagnosis

Cavitary air-space consolidation in ANCA-associated granulomatous vasculitis can be thought to be necrotizing bacterial pneumonia. A secondary infection sometimes occurs in cavitary nodules (43,47). This complication causes progressive consolidation or new air-fluid levels in pre-existing cavities, mimicking progression of ANCA-associated granulomatous vasculitis. If cavitary nodules are multiple, the presence of nodules can raise the possibility of cavitary metastases or the multinodular form of bronchioloalveolar cell carcinoma. Septic pneumonia, fungal pneumonia, pulmonary tuberculosis, or multifocal parenchymal infarctions should also be considered in the differential diagnosis.

Churg-Strauss Syndrome

Clinical and Histologic Findings

The clinical presentation of CSS is distinct from the presentation of ANCA-associated granulomatous vasculitis or microscopic polyangiitis. The annual incidence of CSS is an estimated 0.24 case per 100000 (36). The mean age of onset is 38 years. Asthma is essentially universal in CSS, and virtually all patients have eosinophilia (52–54). Cardiac involvement occurs in 13%–47% of cases and is a major cause of mortality (52). Eosinophil infiltration in the endocardium and cardiac toxin released from eosinophils induce endocardial thickening and thrombus formation and myocardial dysfunction (53). These cardiac changes are best detected at cardiac MR imaging (52–54). As compared with ANCA-associated granulomatous vasculitis and microscopic polyangiitis, peripheral nerve involvement is more common and pulmonary hemorrhage and glomerulonephritis are much less common (1,3). Approximately 40%–75% of patients have ANCA, usually perinuclear. The diagnosis of CSS is established in patients with evidence of vasculitis at biopsy plus at least four of the following criteria: *(a)* asthma, *(b)* blood eosinophilia (>10% of the total white blood cell count), *(c)* mono- or polyneuropathy, *(e)* nonfixed pulmonary infiltrates, *(f)* sinus abnormality, or *(g)* extravascular eosinophils as seen on a biopsy specimen. These diagnostic criteria have shown a sensitivity of 85% and a specificity of near 100% (54).

CSS manifests with a spectrum of histologic changes in the lungs, including asthmatic bronchitis, eosinophilic pneumonia, extravascular granulomas, and necrotizing vasculitis (55). Asthmatic bronchitis shows goblet cell hyperplasia, basement membrane thickening, smooth muscle hyperplasia, and eosinophils in the bronchial walls, along with intraluminal mucinous exudates containing eosinophils. Eosinophilic pneumonia is composed of a mixture of eosinophils and macrophages that fill alveolar spaces. Eosinophilic abscesses and parenchymal necrosis are often seen. CSS granulomas are usually necrotizing and have a border of palisading histiocytes and multinucleated giant cells. The vasculitis affects arterioles and venules. Numerous eosinophils with chronic inflammatory cells are seen in the vessel walls. The vasculitis may show granulomatous features or contain numerous giant cells (55).

Imaging Findings

Although CSS is characterized by systemic vasculitis involving multiple organs, upper airway disease and pulmonary abnormalities are most common and occur in approximately 70% of patients (56,57). The most common radiographic findings consist of transient, patchy, nonsegmental opacities without predilection for any

Figure 10

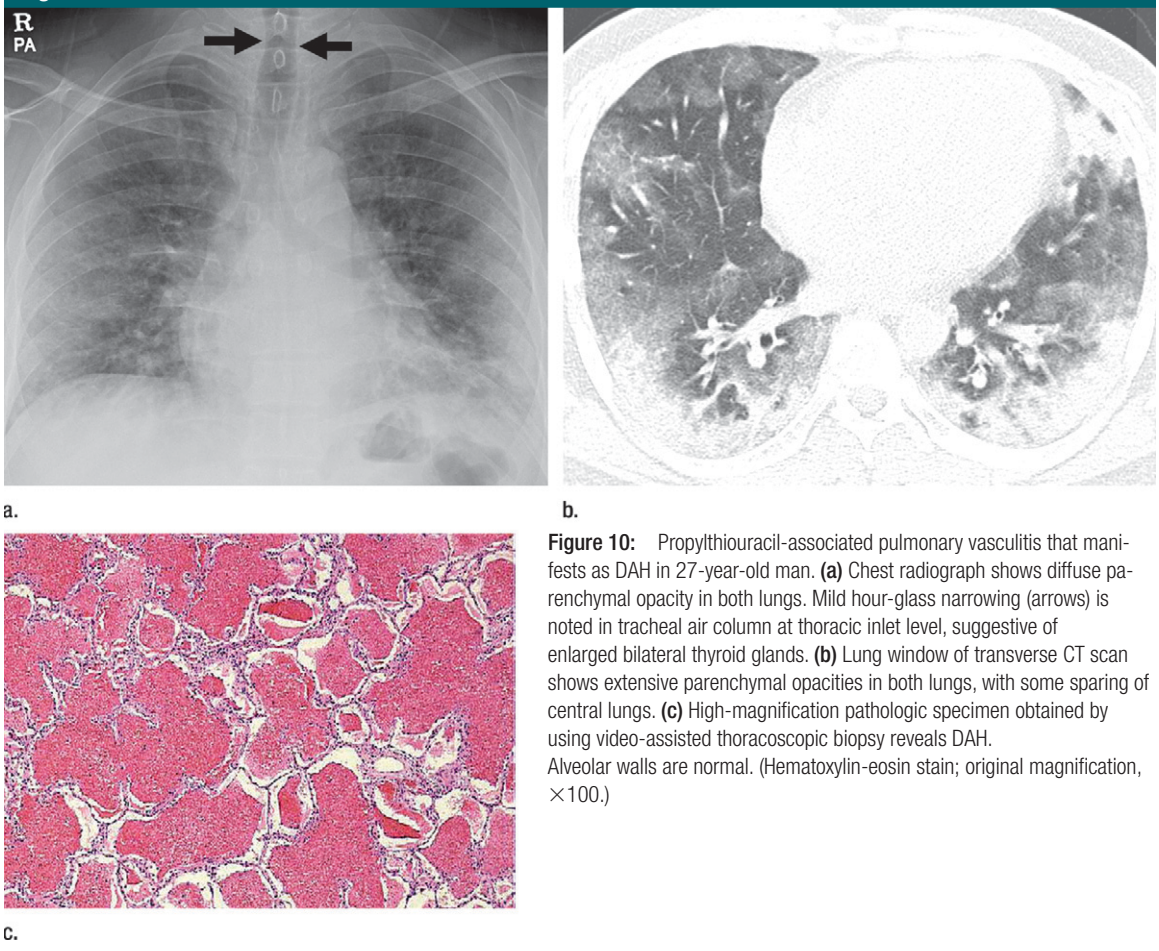

Figure 10: Propylthiouracil-associated pulmonary vasculitis that manifests as DAH in 27-year-old man. **(a)** Chest radiograph shows diffuse parenchymal opacity in both lungs. Mild hour-glass narrowing (arrows) is noted in tracheal air column at thoracic inlet level, suggestive of enlarged bilateral thyroid glands. **(b)** Lung window of transverse CT scan shows extensive parenchymal opacities in both lungs, with some sparing of central lungs. **(c)** High-magnification pathologic specimen obtained by using video-assisted thoracoscopic biopsy reveals DAH. Alveolar walls are normal. (Hematoxylin-eosin stain; original magnification, ×100.)

lung zone (Fig 6). The presence of small noncavitary nodules or diffuse reticular opacities has also been reported (56,58) (Fig 7).

In earlier reports, parenchymal opacities were considered as the predominant pattern of lung abnormality at CT (59,60) (Fig 6). Currently, an airway pattern of lung abnormality is also considered an important CT thoracic manifestation of the disease (61) (Fig 7). Common abnormalities depicted on thin-section CT images consist of small nodules (63%), GGO (53%), bronchial wall thickening (53%) or dilatation (53%), consolidation (42%), interlobular septal thickening (42%), and mosaic perfusion (47%). Small nodules (<10 mm in diameter) are centrilobular within the secondary pulmonary lobule and histopathologically correlate with areas of dense eosinophilic and lymphocytic infiltration in the bronchiolar walls and patchy areas of capillaritis in alveolar walls (61) (Fig 7). The area of consolidation corresponds histopathologically to the area of eosinophilic or granulomatous inflammation (with or without vasculitis) predominantly in the alveoli and alveolar walls (60,61) (Fig 6). Parenchymal lesions that include small nodules, GGOs, consolidation, and tree-in-bud opacities do not show any zonal predominance, except for interlobular septal thickening that has subpleural predominance (61). Interlobular septal thickening may be histopathologically caused by septal edema, eosinophilic infiltration, and mild fibrosis (60). Unilateral or bilateral pleural effusion is seen at CT in up to 50% of cases and may be caused by cardiomyopathy or eosinophilic pleuritis (60,62,63).

Differential Diagnosis

CSS should be differentiated from other eosinophilic lung diseases, including simple pulmonary eosinophilia (Loffler syndrome) and chronic eosinophilic pneumonia. However, these other eosinophilic lung diseases often cause diagnostic problems histopathologically, as well as radiologically, because findings suggestive of vasculitis are not easily demonstrated in the area of eosinophilic infiltration and granulomatous inflammation (59,60,63). The airway pattern of centrilobular small nodules or nodular GGO should be differentiated from various conditions, including subacute hypersensitivity pneumonitis, metastatic calcification, microscopic polyangiitis, SLE, and respiratory bronchiolitis-interstitial lung disease (64).

Figure 11

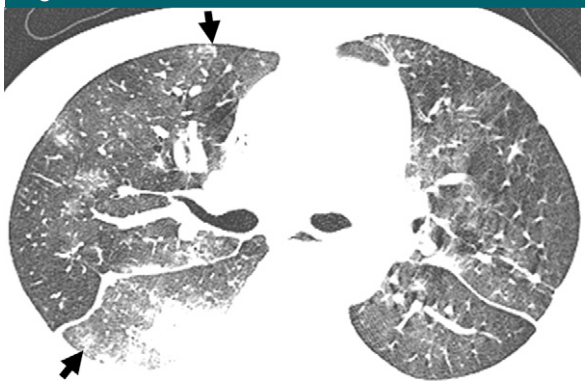

Figure 11: SLE and DAH in 30-year-old woman with a perinuclear ANCA– positive serologic test complaining of hemoptysis. There is decreased serum hemoglobin level (6.9 g/dL [69 g/L]). Lung window image of thin-section CT at level of main bronchi shows extensive opacities in both lungs representing pulmonary hemorrhage. Note small centrilobular nodules (arrows).

Figure 12

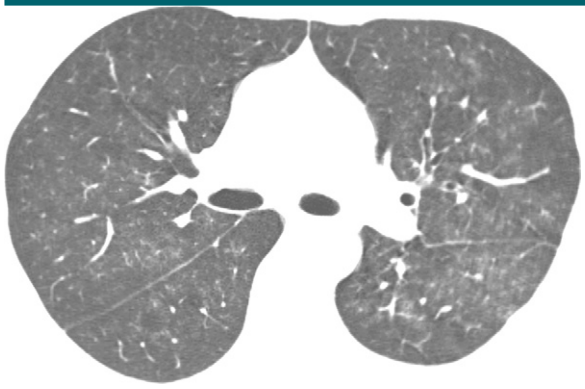

Figure 12: Goodpasture syndrome in 41-year-old man. Lung window of thin-section CT scan at level of main bronchi shows diffuse GGO in both lungs representing DAH. (Image courtesy of Nestor L. Muller, MD, PhD.)

Microscopic Polyangiitis

Microscopic polyangiitis is a systemic necrotizing vasculitis of small vessels without granulomatous inflammation. The annual incidence of microscopic polyangiitis is estimated as 0.36 case per 100 000 (36).

Clinical and Histologic Findings

Pulmonary hemorrhage and neutrophilic capillaritis are the most common findings. Pulmonary capillaritis on biopsy specimens is often difficult to recognize, because capillaritis areas within thickened alveolar walls are sparsely distributed. At closer examination, capillaritis can be identified by the thickening of the alveolar walls with many neutrophils and nuclear dusts (65) (Fig 8). The neutrophils often show karyorrhexis (fragmentation of the nucleus of a cell). Alveolar hemorrhage consists of both hemosiderin and fresh blood admixed with karyorrhectic cell debris (66).

The characteristic clinical manifestation of microscopic polyangiitis is a long prodromal phase of symptoms such as fever and weight loss, followed by the development of rapidly progressive glomerulonephritis (Fig 8). The disease may affect many organ systems, including the kidneys, peripheral nervous system, skin, and lungs. Microscopic polyangiitis is the most common cause of pulmonary-renal syndrome (67). The median age of onset is 50 years. Glomerulonephritis is observed in 90% of patients. Pulmonary involvement occurs in approximately 25%–50% of patients (5,66). Involvement of the sinuses, upper airway, or the eyes is uncommon. Perinuclear ANCA is positive in 40%–80% of patients. The Chapel Hill consensus conference recognized microscopic polyangiitis as its own entity (15) (Fig 1). Microscopic polyangiitis is clinically different from polyarteritis nodosa, which is a vasculitis of medium-sized vessels and where pulmonary artery involvement is very rare (68,69).

Imaging Findings

The radiologic features reflect DAH (Fig 8). Patients with a normal chest radiograph may have bilateral diffuse GGO as depicted on CT images (70). The use of thin-section CT is recommended in patients with clinically suspected pulmonary hemorrhage, notably in patients with an acutely deteriorating renal function, regardless of the presence of normal or questionable radiographic abnormalities. More commonly, every patient with hemoptysis should undergo a CT to exclude other causes of hemoptysis, including the possibility of bronchiectasis, an endobronchial or endotracheal tumor, or an infection that may cause hemoptysis. Repeated hemorrhage in microscopic polyangiitis may lead to interstitial fibrosis in a small number of patients. The presence of pulmonary fibrosis appears to be associated with a poor prognosis (18). The main differential diagnosis that may cause pulmonary and renal manifestations includes Goodpasture syndrome, ANCA-associated granulomatous vasculitis, and SLE (69,70).

Imaging Findings of DAH

The radiographic features of DAH consist of patchy, bilateral air-space opacities (71) (Figs 8–10). DAH is usually seen with extensive bilateral air-space consolidation and GGO, but may be more prominent in the perihilar areas and in the middle and lower lung zones, sparing the lung apices and costophrenic angles (71) (Fig 8).

The most common CT features of DAH are bilateral GGOs and consolidation (Figs 8–12). The lesions are diffuse in the upper and lower lobes in approximately three-fourths of patients (Figs 9–12) or are localized in the lower part of the lungs in 25% of patients (70) (Fig 8). Typically, the halo sign may be seen with parenchymal nodules or masses and consolidation on CT scans, representing

Figure 13

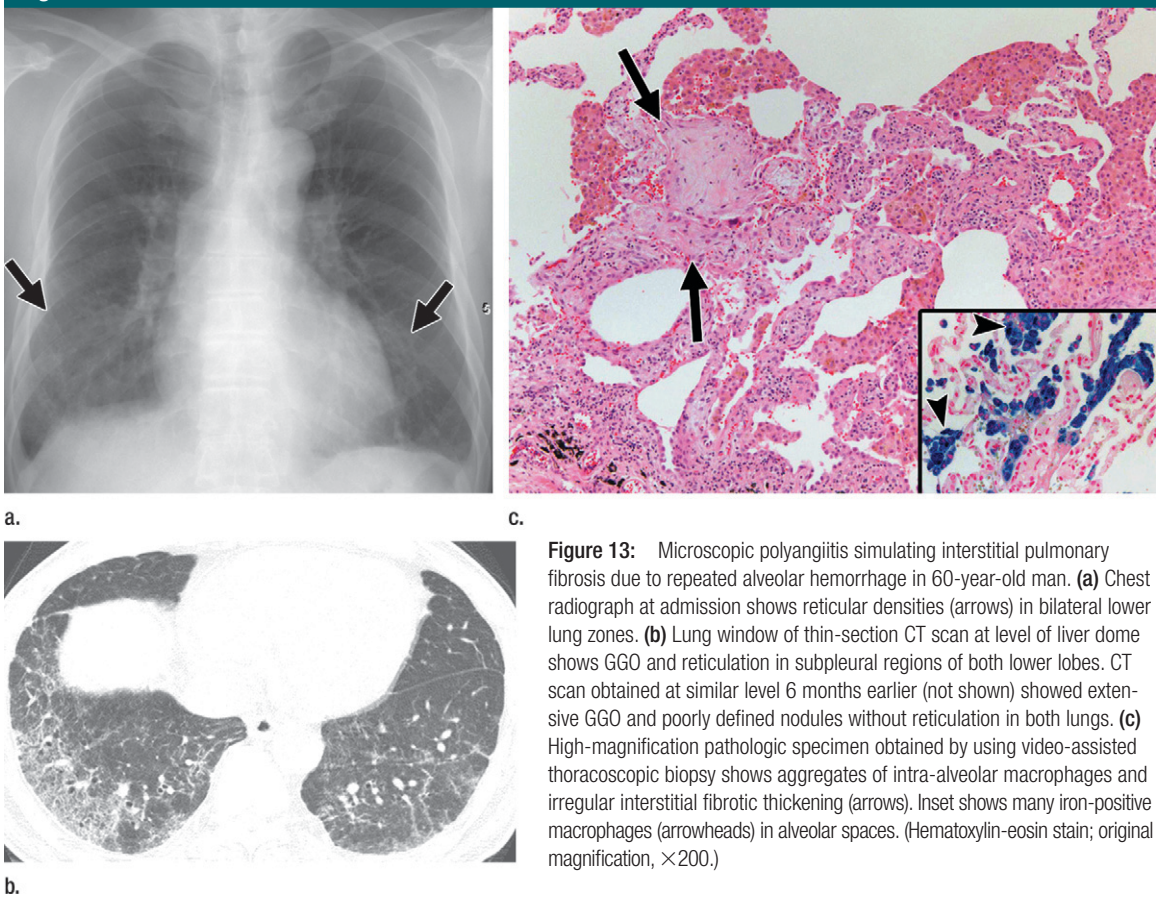

Figure 13: Microscopic polyangiitis simulating interstitial pulmonary fibrosis due to repeated alveolar hemorrhage in 60-year-old man. **(a)** Chest radiograph at admission shows reticular densities (arrows) in bilateral lower lung zones. **(b)** Lung window of thin-section CT scan at level of liver dome shows GGO and reticulation in subpleural regions of both lower lobes. CT scan obtained at similar level 6 months earlier (not shown) showed extensive GGO and poorly defined nodules without reticulation in both lungs. **(c)** High-magnification pathologic specimen obtained by using video-assisted thoracoscopic biopsy shows aggregates of intra-alveolar macrophages and irregular interstitial fibrotic thickening (arrows). Inset shows many iron-positive macrophages (arrowheads) in alveolar spaces. (Hematoxylin-eosin stain; original magnification, ×200.)

Figure 14

Figure 14: Behçet disease in 31-year-old woman. Mediastinal window of transverse contrast-enhanced CT scan shows aneurysmal dilatation of first branch of left upper lobar pulmonary artery. Note wall thickening (arrows) associated with aneurysm.

the hemorrhagic nature of these parenchymal lesions (47,72) (Fig 8). Smooth interlobular septal thickening becomes superimposed on areas of GGO (a crazy-paving appearance) within 2–3 days. These findings may show improvement in the course of hemorrhage resorption. Additionally, ill-defined centrilobular nodules may be present, reflecting intra-alveolar accumulation of pulmonary macrophages (Fig 11). Nodules have been reported to be uniform in size (1–3 mm in diameter) and are diffusely distributed with no zonal predominance (73). Pleural effusion, small in amount, may occur, but is uncommon (70,74). The air-space lesions histopathologically correlate with pulmonary hemorrhage, both with or without capillaritis (71) (Figs 8, 10).

Typical MR features attributable to paramagnetic properties of hemosiderin in DAH are expected to be observed, with diffusely increased signal intensity on T1-weighted MR images and markedly reduced signal intensity on T2-weighted MR images (75). Pulmonary interstitial fibrosis, probably associated with recurrent hemorrhage, has been occasionally reported in pulmonary vasculitis and DAH (18). CT findings in this group of patients may simulate idiopathic pulmonary fibrosis or nonspecific interstitial pneumonitis by showing honeycombing, reticulation, and traction bronchiectasis (18) (Fig 13).

Henoch-Schonlein Purpura

Henoch-Schonlein purpura refers to the condition of a systemic vasculitis characterized by deposition of immune complexes, including IgA, in the skin and kidneys. It occurs more often in children than in adults. Half of the affected patients are younger than 6 years of age and 90% of patients are younger than 10 years of age. Boys are involved twice as often as girls. The incidence of the disease in children is approximately 20 per 100 000, representing

Figure 15

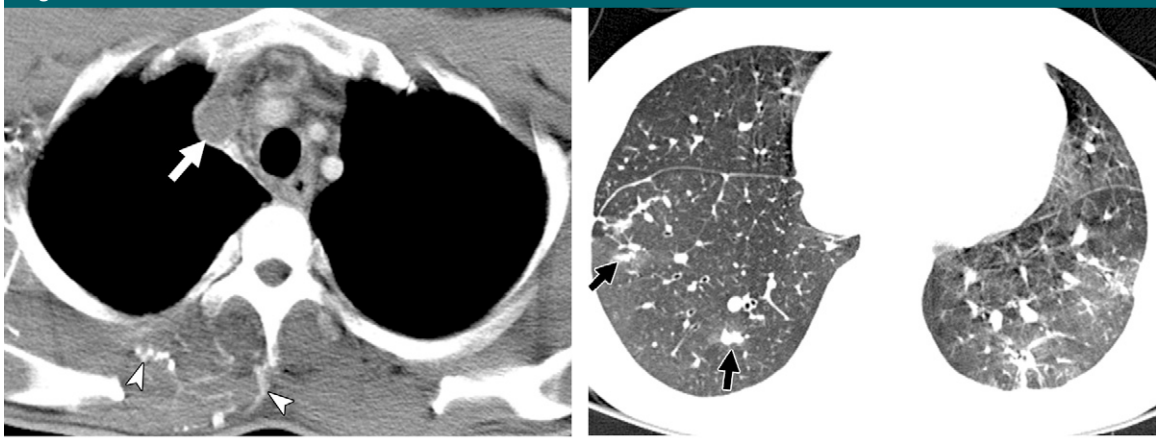

a. b.

Figure 15: Behçet disease in 38-year-old man. **(a)** Mediastinal window of contrast-enhanced CT scan at level of thoracic inlet shows thrombosed superior vena cava (arrow) and chest wall collateral vessel development (arrowheads). **(b)** Lung window of thin-section CT scan at level of suprahepatic inferior vena cava shows nodules and halo sign (arrows) and areas of GGO in both lungs. Nodules are presumed to represent thrombosed pulmonary arteries and GGO pulmonary hemorrhage.

the most common vasculitis in childhood (76,77).

Purpura, arthritis, and abdominal pain are known as the classic triad of Henoch-Schonlein purpura. Purpura occurs in all cases, joint pains and arthritis occur in 80% of cases, and abdominal pain occurs in 62% of involved children. Kidney involvement has been identified in 40% of cases (76).

Pulmonary involvement in Henoch-Schonlein purpura is rare and one of a variety of diseases associated with necrotizing capillaritis. Deposition of antiglomerular basement membrane (renal tubular and glomerular) IgA to the alveolar basement membrane leads to immune complex pneumonitis and leukocytoclastic capillaritis. It occurs more often in adults and commonly manifests as DAH (Fig 9) on imaging studies and occasionally as a pattern of interstitial pulmonary fibrosis (78).

Essential Cryoglobulinemic Vasculitis

Cryoglobulins are immunoglobulins that precipitate when serum is incubated at a temperature lower than the body temperature. Half of patients with cryoglobulinemia have clinical manifestation of systemic vasculitis caused by small-vessel damage as a result of deposition of immune complexes on small vessel walls and following complex activation (79,80). The resulting vasculitis leads to a broad spectrum of clinical features involving the skin, joints, kidneys, and peripheral nerves (79). Pulmonary vasculitis is rare. Approximately 2% (four of 209) of patients with cryoglobulinemic vasculitis have pulmonary vasculitis, which is usually manifested as life-threatening DAH clinically or on imaging studies. The prognosis for patients with pulmonary vasculitis is poor, and almost all patients die of the disease (80).

Cutaneous Leukocytoclastic Angiitis

Cutaneous leukocytoclastic angiitis is a small-vessel, acute-necrotizing, inflammatory disease caused by deposition of immune complexes and characterized clinically by the presence of purpura in the lower extremities (81,82). Abdominal pain, arthralgia, and renal involvement may be accompanied by the purpura. It is of unknown etiology in half of the patients; in the remaining half, it is associated with collagen vascular disease, systemic necrotizing vasculitis, bacterial and viral infections, drug use, or malignancies (81). When the disease manifests with unknown etiology, lung involvement is absent. However, since the disorder is associated with various diseases, pulmonary manifestations depend on lung involvement of associated diseases (eg, collagen vascular disease or systemic necrotizing vasculitis such as ANCA-associated granulomatous vasculitis and CSS) (81,82). Therefore, various patterns of lung abnormalities may be shown on imaging studies when it manifests as an associated disease.

Isolated Pauci-immune Pulmonary Capillaritis

Isolated pauci-immune pulmonary capillaritis rarely causes DAH without clinical, serological, or histologic evidence of an accompanying systemic disease (16). Glomerulonephritis is absent. Serum ANCA test shows negative result. The median age of onset is 30 years. Recurrences of DAH may occur, but the prognosis appears favorable (16).

Behçet Disease

Behçet disease is a chronic systemic vasculitis that occurs predominantly in young men, most commonly along the old silk route (from Japan and China in the Far East to the Mediterranean Sea, including the countries such as Turkey and Iran), and thoracic involvement has

Figure 16

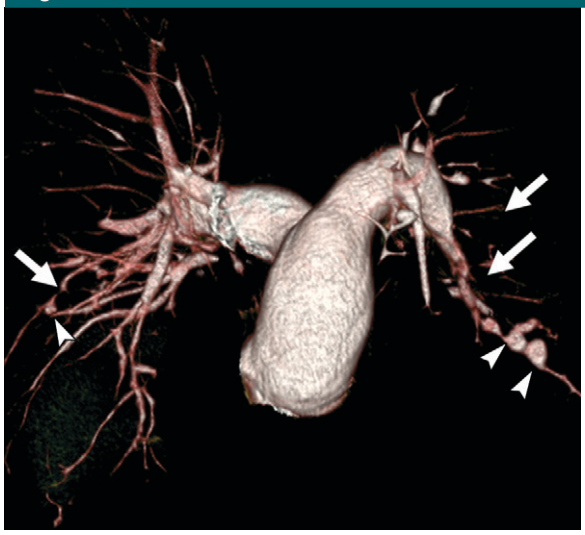

Figure 16: Hughes-Stovin syndrome in 35-year-old man. Three-dimensional volume-rendered CT pulmonary arteriogram shows irregular narrowing and pruned-tree appearance (arrows) of pulmonary arteries, as well as aneurysmal dilatation (arrowheads) of peripheral pulmonary arteries.

been reported in up to 8% of patients with the disease (83). Neither the cause nor the epidemiology of Behçet disease is well known. An immunogenetic mechanism may play an important role in its development (17). Histologic findings of vascular involvement include medial thickening, elastic fiber splitting, and perivascular round cell infiltration (83). The four types of vascular lesions recognized include arterial occlusion, venous occlusion, aneurysms (Figs 14, 15), and varices. The presence of an aneurysm and occlusion are the most common findings (83–85).

In approximately 5% of patients, lymphocytic necrotizing vasculitis of the pulmonary arteries can occur. Pulmonary vasculitis of Behçet disease usually causes pulmonary artery aneurysms, thrombosis, infarction, hemorrhage, and arteriovenous shunts. In cases with hemoptysis, a bleeding aneurysm must be differentiated from thromboembolism to decide about the use of anticoagulants (17,83).

Thoracic manifestation includes aneurysms of the pulmonary artery, pulmonary infarction or hemorrhage, and thrombosis of the superior vena cava. Pulmonary vascular involvement can produce dyspnea, chest pain, cough, or hemoptysis. The natural history is characterized by chronic exacerbations. Because aneurysms evolve rapidly, aneurysm size measurements cannot be used to predict the risk of rupture. Consequently, pulmonary aneurysm formation in untreated patients carries a high mortality rate of 30% within 2 years (84,85).

Radiographic findings include the presence of a lung mass due to aneurysms of pulmonary arteries (Fig 14), wedge-shaped air-space consolidation due to infarction or hemorrhage, and mediastinal widening due to thrombosis of the superior vena cava (Fig 15). Aneurysms in Behçet disease are fusiform to saccular, are commonly multiple in number and bilateral, and are located in the lower lobes or the main pulmonary arteries (86). The use of CT imaging can help characterize disease-induced or therapy-induced changes. Aneurysmal wall thickening represents subadventitial hematoma formation (Fig 14), and perianeurysmal air-space consolidation or GGO is indicative of an impending rupture (87–90). Additional findings include peripheral mosaic perfusion resulting from focal air trapping, thrombotic small-vessel occlusion (Fig 15) or mechanical vascular compression by aneurysms, and organizing or eosinophilic pneumonia (90). Acute arterial hemorrhage is a well-recognized complication of vasculitis, and the rupture of a pulmonary artery into a bronchial lumen or into the parenchyma occurs in up to 50% of patients with pulmonary artery aneurysms (86). There is evidence of complete resolution of up to 75% of aneurysms in patients who receive immunosuppressant treatment (86). Aneurysm regression is usually preceded by thrombus formation, which also disappears after treatment.

Hughes-Stovin Syndrome

Hughes-Stovin syndrome is an exceedingly rare disorder of unknown etiology and is characterized by multiple pulmonary artery aneurysms and peripheral venous thrombosis (91). It causes large-vessel vasculitis that affects pulmonary and frequently bronchial arteries and large systemic veins. It is widely accepted as a "forme frusta" of Behçet disease because, apart from vascular findings, clinical diagnostic criteria of the latter are absent (92). It occurs predominantly in young adult men between 2nd and 4th decade of life. Pulmonary artery aneurysm has been attributed to weakening of vessel walls due to inflammation. Pathologic features include systemic thrombi in the vena cava, cerebral sinuses, or limb veins; pulmonary artery occlusions due to emboli or thrombi; and one or more segmental pulmonary artery aneurysms, frequently associated with bronchial artery aneurysms (93) (Fig 16).

The typical clinical manifestation consists of three phases: a first stage with symptoms of thrombophlebitis, a second stage with formation and enlargement of pulmonary aneurysms, and a third stage with aneurysmal rupture that triggers massive hemoptysis and death (94). The radiologic features are similar to those of Behçet disease. For the differential diagnosis of a pulmonary or bronchial artery aneurysm, pulmonary artery aplasia, trauma, infection, silicosis, and vasculitis (including Behçet disease) should be considered.

Vasculitis Associated with Collagen Vascular Disease

Pulmonary capillaritis can manifest as a complication of a disease course of various

Figure 17

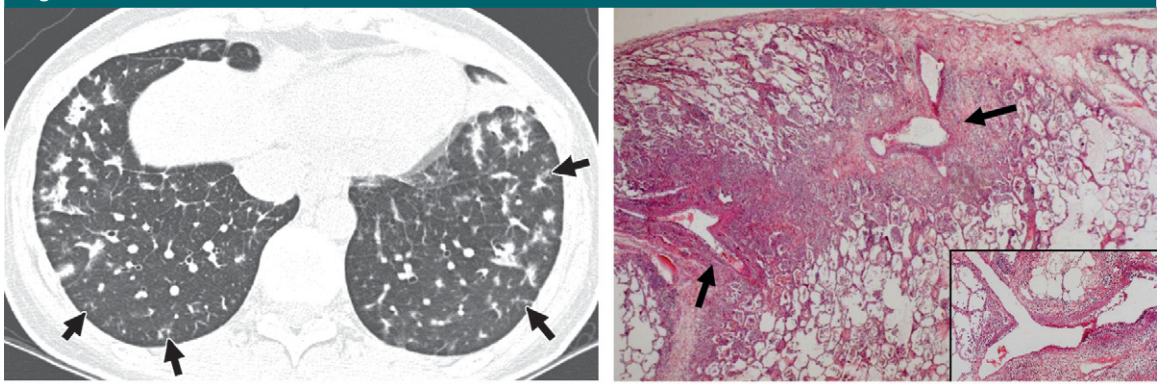

a. b.

Figure 17: Necrotizing vasculitis in 31-year-old woman with SLE. **(a)** Lung window of thin-section CT scan at level of suprahepatic inferior vena cava shows variable-sized nodules and areas of tree-in-bud signs of vascular origin (arrows) in both lungs. **(b)** High-magnification pathologic specimen obtained by using video-assisted thoracoscopic biopsy shows necrotizing vasculitis involving centrilobular arterioles (arrows). Inset shows acute inflammation in centrilobular arterioles with marked edema and fibrinoid necrosis. (Hematoxylin-eosin stain; original magnification, ×100.)

kinds of collagen vascular diseases such as SLE, rheumatoid arthritis, polymyositis, Sjogren syndrome, scleroderma, and primary antiphospholipid syndrome (95).

The lungs and pleura are affected more frequently in SLE (50%–70% of cases) than in other collagen vascular diseases, and lung involvement manifests with diverse pathologic entities (96). SLE vasculitis is immune complex mediated and involves the arterioles and capillaries; necrotizing arteriolitis (much rarer than capillaritis) results in edema and fibrinoid necrosis in the arterioles within the secondary pulmonary lobule, and acute necrotizing capillaritis (more common than arteriolitis) chiefly causes DAH (97). When DAH does occur, it is often seen concomitantly with other pulmonary manifestations of SLE such as acute lupus pneumonitis, pulmonary edema, or pleural effusion.

DAH occurs in 4% of hospitalized patients with SLE, representing 22% of the pulmonary complications of SLE. Typically, patients with DAH present with rapid-onset tachypnea, cough, fever, hypoxia, and hemoptysis while displaying symptoms of generalized SLE vasculitis such as renal failure, arthritis, or rash (97). It is known that the presence of DAH should exclude scleroderma, rheumatoid arthritis, and dermatomyositis or polymyositis (98). However, DAH has been reported in a small number of patients with mixed connective tissue disease, and it has occurred predominantly in association with glomerulonephritis (99,100). Similarly, DAH has been reported in a small number of cases of rheumatoid arthritis (101).

Necrotizing vasculitis in SLE that mainly involves arterioles within the secondary pulmonary lobules may appear with centrilobular small nodules or tree-in-bud opacities of vascular origin at CT (Fig 17). In SLE, pulmonary hypertension occurs in 0.5%–14% of patients (102). The above-mentioned necrotizing vasculitis may be a factor in pulmonary hypertension in SLE patients. Recurrent thromboembolic disease, bland vasculopathy as in primary pulmonary hypertension, and interstitial pulmonary fibrosis and hypoxia may also contribute to pulmonary arterial hypertension (103).

Drug- and Foreign Material–induced Pulmonary Vasculitis

Propylthiouracil, gemcitabine, diphenylhydantoin, transretinoic acid, and crack cocaine may cause pulmonary capillaritis and DAH (Fig 10) (1,104–107). Immune mechanisms that include ANCA-related vasculitis have been regarded as responsible for the underlying pathogenesis of such drug-induced pulmonary vasculitis. Imaging studies usually depict the findings of DAH (104–107).

Foreign materials such as talc, starch, cellulose, and maltose, used as filler for tablets and capsules taken orally, may be injected in suspension by drug abusers and can cause a foreign body granulomatous reaction that is centered on arterioles. A chest radiograph may show small nodules and a CT scan can show centrilobular small nodules or vascular tree-in-bud opacities within the secondary pulmonary lobule. Conglomeration and fibrosis of nodules may lead to progressive massive fibrosis (10,108,109).

Goodpasture Syndrome

The clinical triad of circulating antiglomerular basement membrane antibody, DAH, and glomerulonephritis characterizes Goodpasture syndrome. It usually occurs in young adult men, although the age range is wide. Presenting symptoms are usually related to respiratory rather than renal involvement (71).

The syndrome is caused by immune antibody deposits with antiglomerular basement membrane antibody. A demonstration by immunofluorescence of the linear deposition of IgG on glomerular basement membranes seen at a renal

Figure 18

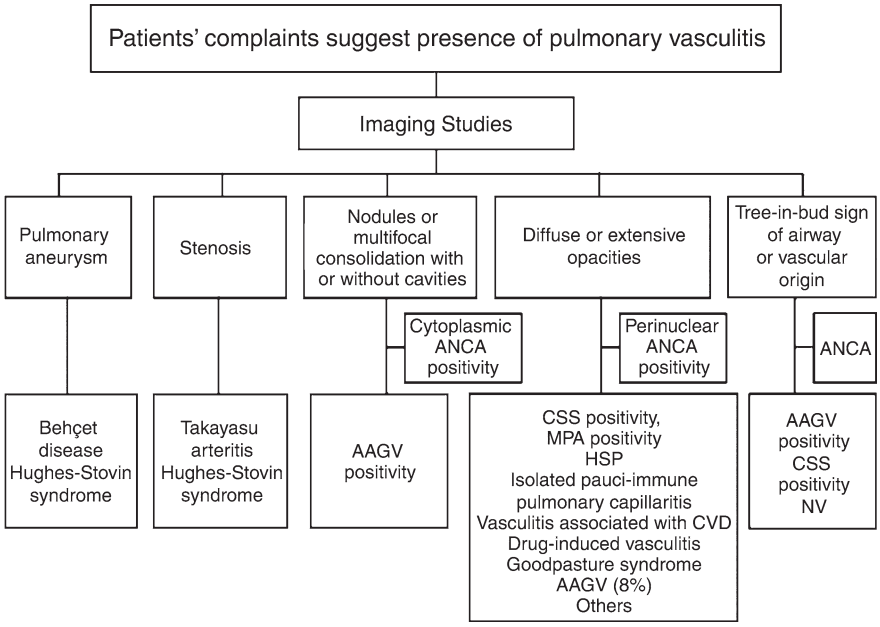

Figure 18: Flowchart shows the approach for reaching a specific diagnosis of pulmonary vasculitis in patients with DAH, glomerulonephritis, upper respiratory tract disease, mononeuritis multiplex, multisystemic disease, or palpable purpura. Cytoplasmic ANCA positivity allows one to make a confident diagnosis of Wegener granulomatosis and perinuclear ANCA positivity suggests presence of CSS or MPA. *AAGV* = ANCA-associated granulomatous vasculitis, *CVD* = collagen vascular disease, *HSP* = Henoch-Schonlein purpura, *MPA* = microscopic polyangiitis, *NV* = necrotizing vasculitis involving pulmonary arterioles (in SLE and foreign-material induced vasculitis).

biopsy can be used to make the diagnosis of Goodpasture syndrome (71). Goodpasture syndrome usually shows intra-alveolar hemorrhage or presence of hemosiderin-laden macrophages. Although neutrophilic capillaritis is usually not extensive, it may be seen. The alveolar septa can be mildly thickened by interstitial fibrosis. Linear deposition of IgG and complement can be demonstrated in the basement membranes of the alveoli (110). As seen on CT images, DAH is the key feature of pulmonary involvement (Fig 12) and typically resolves within a few days. On rare occasions, the pulmonary changes may be isolated without renal involvement (110).

IgA Nephropathy-associated Capillaritis

Pulmonary capillaritis is a rare systemic manifestation of IgA nephropathy, where renal and pulmonary manifestations usually occur concurrently (111,112). Therefore, the two manifestations are considered the same underlying immune process. However, in IgA nephropathy, pulmonary capillaritis can occur at a time independent of kidney disease, long after the renal manifestations have resolved. The underlying mechanism is an immune complex (antiglomerular basement membrane IgA)-mediated pulmonary injury, a variation of Henoch-Schonlein purpura capillaritis (111,112). Imaging findings are identical to those of DAH.

Conclusion

Clinical symptoms and radiologic signs suggestive of pulmonary vasculitis include DAH, acute glomerulonephritis, upper airway disease, imaging findings of lung nodules or cavitary lesions, mononeuritis multiplex, multisystemic disease, and palpable purpura. In such a clinical setting, we recommend that patients undergo a cytoplasmic ANCA and perinuclear ANCA study. A cytoplasmic ANCA study is both sensitive and specific for ANCA-associated granulomatous vasculitis in the appropriate clinical setting. A perinuclear ANCA study is neither sensitive nor specific, but it is suggestive of the presence of CSS and microscopic polyangiitis. Main patterns of pulmonary abnormalities include pulmonary artery aneurysm, stenosis, nodules or multifocal consolidation with or without cavity, diffuse or extensive opacities, and tree-in-bud sign. Radiologic findings depend on the level of pulmonary vessels involved. Diseases of elastic arteries show aneurismal dilatation with or without intraluminal thrombosis or vascular stenosis with inflammatory wall thickening and luminal narrowing, whereas diseases of muscular arteries or arterioles usually manifest as cavitating or noncavitating nodules or multifocal consolidation along the bronchovascular bundles. Vasculitis involving capillaries or arterioles usually demonstrates DAH or small centrilobular nodules and tree-in-bud signs of vascular origin. However, the differential diagnosis from other nonvascular diseases is not easy; therefore, it is essential to integrate clinical, laboratory, and imaging findings to make a specific diagnosis of pulmonary vasculitides (Fig 18).

References

1. Brown KK. Pulmonary vasculitis. Proc Am Thorac Soc 2006;3(1):48–57.
2. Hansell DM. Small-vessel diseases of the lung: CT-pathologic correlates. Radiology 2002;225(3):639–653.
3. Frankel SK, Cosgrove GP, Fischer A, Meehan RT, Brown KK. Update in the diagnosis and management of pulmonary vasculitis. Chest 2006;129(2):452–465.
4. Hagen EC, Daha MR, Hermans J, et al. Diagnostic value of standardized assays for anti-neutrophil cytoplasmic antibodies in idiopathic systemic vasculitis. EC/BCR Project for ANCA Assay Standardization. Kidney Int 1998;53(3):743–753.
5. Guillevin L, Durand-Gasselin B, Cevallos R, et al. Microscopic polyangiitis: clinical and laboratory findings in eighty-five patients. Arthritis Rheum 1999;42(3):421–430.
6. Mulder AH, Horst G, van Leeuwen MA, Limburg PC, Kallenberg CG. Antineutrophil

cytoplasmic antibodies in rheumatoid arthritis: characterization and clinical correlations. Arthritis Rheum 1993;36(8):1054–1060.

7. Schnabel A, Csernok E, Isenberg DA, Mrowka C, Gross WL. Antineutrophil cytoplasmic antibodies in systemic lupus erythematosus: prevalence, specificities, and clinical significance. Arthritis Rheum 1995;38(5):633–637.
8. Kerr GS, Fleisher TA, Hallahan CW, Leavitt RY, Fauci AS, Hoffman GS. Limited prognostic value of changes in antineutrophil cytoplasmic antibody titers in patients with Wegener's granulomatosis. Adv Exp Med Biol 1993;336:411–414.
9. Ara J, Mirapeix E, Rodriguez R, Saurina A, Darnell A. Relationship between ANCA and disease activity in small vessel vasculitis patients with anti-MPO ANCA. Nephrol Dial Transplant 1999;14(7):1667–1672.
10. Lee KS, Kim TS, Han J, et al. Diffuse micronodular lung disease: HRCT and pathologic findings. J Comput Assist Tomogr 1999;23(1):99–106.
11. Seo JB, Im J-G, Chung JW, et al. Pulmonary vasculitis: the spectrum of radiological findings. Br J Radiol 2000;73(875):1224–1231.
12. Ravenel JG, McAdams HP. Pulmonary vasculitis: CT features. Semin Respir Crit Care Med 2003;24(4):427–436.
13. Peachell MB, Muller NL. Pulmonary vasculitis. Semin Respir Crit Care Med 2004;25(5):483–489.
14. Marten K, Schnyder P, Schirg E, Prokop M, Rummeny EJ, Engelke C. Pattern-based differential diagnosis in pulmonary vasculitis using volumetric CT. AJR Am J Roentgenol 2005;184(3):720–733.
15. Jennette JC, Falk RJ, Andrassy K, et al. Nomenclature of systemic vasculitides: proposal of an international consensus conference. Arthritis Rheum 1994;37(2):187–192.
16. Jennings CA, King TE Jr, Tuder R, Cherniack RM, Schwarz MI. Diffuse alveolar hemorrhage with underlying isolated, pauci-immune pulmonary capillaritis. Am J Respir Crit Care Med 1997;155(3):1101–1109.
17. Jennette JC, Falk RJ. New insight into the pathogenesis of vasculitis associated with antineutrophil cytoplasmic autoantibodies. Curr Opin Rheumatol 2008;20(1):55–60.
18. Eschun GM, Mink SN, Sharma S. Pulmonary interstitial fibrosis as a presenting manifestation in perinuclear antineutrophilic cytoplasmic antibody microscopic polyangiitis. Chest 2003;123(1):297–301.
19. Nathani N, Little MA, Kunst H, Wilson D, Thickett DR. Churg-Strauss syndrome and leukotriene antagonist use: a respiratory perspective. Thorax 2008;63(10):883–888.
20. Cojocaru M, Cojocaru IM, Iacob SA. Prevalence of anti-neutrophil cytoplasmic antibodies in patients with chronic hepatitis C infection associated mixed cryoglobulinemia. Rom J Intern Med 2006;44(4):427–431.
21. Zholudev A, Zurakowski D, Young W, Leichtner A, Bousvaros A. Serologic testing with ANCA, ASCA, and anti-OmpC in children and young adults with Crohn's disease and ulcerative colitis: diagnostic value and correlation with disease phenotype. Am J Gastroenterol 2004;99(11):2235–2241.
22. Seko Y. Giant cell and Takayasu arteritis. Curr Opin Rheumatol 2007;19(1):39–43.
23. Kobayashi Y, Numano F. 3. Takayasu arteritis. Intern Med 2002;41(1):44–46.
24. Johnston SL, Lock RJ, Gompels MM. Takayasu arteritis: a review. J Clin Pathol 2002;55(7):481–486.
25. Matsubara O, Yoshimura N, Tamura A, et al. Pathological features of the pulmonary artery in Takayasu arteritis. Heart Vessels Suppl 1992;718–25.
26. Yamato M, Lecky JW, Hiramatsu K, Kohda E. Takayasu arteritis: radiographic and angiographic findings in 59 patients. Radiology 1986;161(2):329–334.
27. Rizzi R, Bruno S, Stellacci C, Dammacco R. Takayasu's arteritis: a cell-mediated large-vessel vasculitis. Int J Clin Lab Res 1999;29(1):8–13.
28. Park JH, Chung JW, Im J-G, Kim SK, Park YB, Han MC. Takayasu arteritis: evaluation of mural changes in the aorta and pulmonary artery with CT angiography. Radiology 1995;196(1):89–93.
29. Desai MY, Stone JH, Foo TK, Hellmann DB, Lima JA, Bluemke DA. Delayed contrast-enhanced MRI of the aortic wall in Takayasu's arteritis: initial experience. AJR Am J Roentgenol 2005;184(5):1427–1431.
30. Choe YH, Han BK, Koh EM, Kim DK, Do YS, Lee WR. Takayasu's arteritis: assessment of disease activity with contrast-enhanced MR imaging. AJR Am J Roentgenol 2000;175(2):505–511.
31. Schmidt WA, Blockmans D. Use of ultrasonography and positron emission tomography in the diagnosis and assessment of large-vessel vasculitis. Curr Opin Rheumatol 2005;17(1):9–15.
32. Matsunaga N, Hayashi K, Sakamoto I, Ogawa Y, Matsumoto T. Takayasu arteritis: protean radiologic manifestations and diagnosis. RadioGraphics 1997;17(3):579–594.
33. Canyigit M, Peynircioglu B, Hazirolan T, et al. Imaging characteristics of Takayasu arteritis. Cardiovasc Intervent Radiol 2007;30(4):711–718.
34. Woywodt A, Matteson EL. Wegener's granulomatosis: probing the untold past of the man behind the eponym. Rheumatology (Oxford) 2006;45(10):1303–1306.
35. Lamprecht P, Gross WL. Wegener's granulomatosis. Herz 2004;29(1):47–56.
36. Bosch X, Guilabert A, Espinosa G, Mirapeix E. Treatment of antineutrophil cytoplasmic antibody associated vasculitis: a systematic review. JAMA 2007;298(6):655–669.
37. Travis WD, Hoffman GS, Leavitt RY, Pass HI, Fauci AS. Surgical pathology of the lung in Wegener's granulomatosis: review of 87 open lung biopsies from 67 patients. Am J Surg Pathol 1991;15(4):315–333.
38. Yousem SA. Bronchocentric injury in Wegener's granulomatosis: a report of five cases. Hum Pathol 1991;22(6):535–540.
39. Yousem SA, Lombard CM. The eosinophilic variant of Wegener's granulomatosis. Hum Pathol 1988;19(6):682–688.
40. Uner AH, Rozum-Slota B, Katzenstein AL. Bronchiolitis obliterans-organizing pneumonia (BOOP)-like variant of Wegener's granulomatosis: a clinicopathologic study of 16 cases. Am J Surg Pathol 1996;20(7):794–801.
41. Travis WD, Colby TV, Lombard C, Carpenter HA. A clinicopathologic study of 34 cases of diffuse pulmonary hemorrhage with lung biopsy confirmation. Am J Surg Pathol 1990;14(12):1112–1125.
42. Leavitt RY, Fauci AS, Bloch DA, et al. The American College of Rheumatology 1990 criteria for the classification of Wegener's granulomatosis. Arthritis Rheum 1990;33(8):1101–1107.
43. Aberle DR, Gamsu G, Lynch D. Thoracic manifestations of Wegener granulomatosis: diagnosis and course. Radiology 1990;174(3 pt 1):703–709.
44. Kim SJ, Lee KS, Ryu YH, et al. Reversed halo sign on high-resolution CT of cryptogenic organizing pneumonia: diagnostic implications. AJR Am J Roentgenol 2003;180(5):1251–1254.
45. Cordier JF, Valeyre D, Guillevin L, Loire R, Brechot JM. Pulmonary Wegener's granulomatosis: a clinical and imaging study of 77 cases. Chest 1990;97(4):906–912.
46. Reuter M, Schnabel A, Wesner F, et al. Pulmonary Wegener's granulomatosis: correlation between high-resolution CT findings and clinical scoring of disease activity. Chest 1998;114(2):500–506.

47. Lee KS, Kim TS, Fujimoto K, et al. Thoracic manifestation of Wegener's granulomatosis: CT findings in 30 patients. Eur Radiol 2003;13(1):43–51.

48. Lohrmann C, Uhl M, Kotter E, Burger D, Ghanem N, Langer M. Pulmonary manifestations of wegener granulomatosis: CT findings in 57 patients and a review of the literature. Eur J Radiol 2005;53(3):471–477.

49. Attali P, Begum R, Ban Romdhane H, Valeyre D, Guillevin L, Brauner MW. Pulmonary Wegener's granulomatosis: changes at follow-up CT. Eur Radiol 1998;8(6):1009–1113.

50. Pretorius ES, Stone JH, Hellmann DB, Fishman EK. Wegener's granulomatosis: spectrum of CT findings in diagnosis, disease progression, and response to therapy. Crit Rev Diagn Imaging 2000;41(4): 279–313.

51. Pretorius ES, Stone JH, Hellman DB, Fishman EK. Wegener's Granulomatosis: CT evolution of pulmonary parenchymal findings in treated disease. Crit Rev Comput Tomogr 2004;45(1):67–85.

52. Keogh KA, Specks U. Churg-Strauss syndrome: clinical presentation, antineutrophil cytoplasmic antibodies, and leukotriene receptor antagonists. Am J Med 2003;115(4):284–290.

53. Val-Bernal JF, Mayorga M, García-Alberdi E, Pozueta JA. Churg-Strauss syndrome and sudden cardiac death. Cardiovasc Pathol 2003;12(2):94–97.

54. Keogh KA, Specks U. Churg-Strauss syndrome. Semin Respir Crit Care Med 2006;27(2):148–157.

55. Katzenstein AL. Diagnostic features and differential diagnosis of Churg-Strauss syndrome in the lung: a review. Am J Clin Pathol 2000;114(5):767–772.

56. Lanham JG, Elkon KB, Pusey CD, Hughes GR. Systemic vasculitis with asthma and eosinophilia: a clinical approach to the Churg-Strauss syndrome. Medicine (Baltimore) 1984;63(2):65–81.

57. Guillevin L, Cohen P, Gayraud M, Lhote F, Jarrousse B, Casassus P. Churg-Strauss syndrome: clinical study and long-term follow-up of 96 patients. Medicine (Baltimore) 1999;78(1):26–37.

58. Kim Y, Lee KS, Choi DC, Primack SL, Im JG. The spectrum of eosinophilic lung disease: radiologic findings. J Comput Assist Tomogr 1997;21(6):920–930.

59. Worthy SA, Müller NL, Hansell DM, Flower CD. Churg-Strauss syndrome: the spectrum of pulmonary CT findings in 17 patients. AJR Am J Roentgenol 1998;170(2):297–300.

60. Silva CI, Müller NL, Fujimoto K, Johkoh T, Ajzen SA, Churg A. Churg-Strauss syndrome: high resolution CT and pathologic findings. J Thorac Imaging 2005;20(2):74–80.

61. Kim YK, Lee KS, Chung MP, et al. Pulmonary involvement in Churg-Strauss syndrome: an analysis of CT, clinical, and pathologic findings. Eur Radiol 2007;17(12):3157–3165.

62. Choi YH, Im J-G, Han BK, Kim JH, Lee KY, Myoung NH. Thoracic manifestation of Churg-Strauss syndrome: radiologic and clinical findings. Chest 2000;117(1):117–124.

63. Johkoh T, Müller NL, Akira M, et al. Eosinophilic lung diseases: diagnostic accuracy of thin-section CT in 111 patients. Radiology 2000;216(3):773–780.

64. Okada F, Ando Y, Yoshitake S, et al. Clinical/pathologic correlations in 553 patients with primary centrilobular findings on high-resolution CT scan of the thorax. Chest 2007;132(6):1939–1948.

65. Jennette JC, Thomas DB, Falk RJ. Microscopic polyangiitis (microscopic polyarteritis). Semin Diagn Pathol 2001;18(1):3–13.

66. Jennette JC, Falk RJ. Small-vessel vasculitis. N Engl J Med 1997;337(21):1512–1523.

67. Niles JL, Böttinger EP, Saurina GR, et al. The syndrome of lung hemorrhage and nephritis is usually an ANCA-associated condition. Arch Intern Med 1996;156(4):440–445.

68. Pagnoux C, Guilpain P, Guillevin L. Microscopic polyangiitis. [in French]. Presse Med 2007;36(5 pt 2):895–901.

69. Collins CE, Quismorio FP Jr. Pulmonary involvement in microscopic polyangiitis. Curr Opin Pulm Med 2005;11(5):447–451.

70. Lauque D, Cadranel J, Lazor R, et al. Microscopic polyangiitis with alveolar hemorrhage: a study of 29 cases and review of the literature. Groupe d'Etudes et de Recherche sur les Maladies "Orphelines" Pulmonaires (GERM"O"P). Medicine (Baltimore) 2000;79(4):222–233.

71. Primack SL, Miller RR, Müller NL. Diffuse pulmonary hemorrhage: clinical, pathologic, and imaging features. AJR Am J Roentgenol 1995;164(2):295–300.

72. Primack SL, Hartman TE, Lee KS, Müller NL. Pulmonary nodules and the CT halo sign. Radiology 1994;190(2):513–515.

73. Cheah FK, Sheppard MN, Hansell DM. Computed tomography of diffuse pulmonary haemorrhage with pathological correlation. Clin Radiol 1993;48(2):89–93.

74. Gülbay BE, Celik G, Kumbasar O, Gülbay M, Alper D, Tulunay O. Microscopic polyangiitis with unusual lung involvement. Respirology 2005;10(5):678–681.

75. Rubin GD, Edwards DK 3rd, Reicher MA, Doemeny JM, Carson SH. Diagnosis of pulmonary hemosiderosis by MR imaging. AJR Am J Roentgenol 1989;152(3):573–574.

76. Saulsbury FT. Henoch-Schönlein purpura. Curr Opin Rheumatol 2001;13(1):35–40.

77. Gardner-Medwin JM, Dolezalova P, Cummins C, Southwood TR. Incidence of Henoch-Schönlein purpura, Kawasaki disease, and rare vasculitides in children of different ethnic origins. Lancet 2002;360(9341): 1197–1202.

78. Nadrous HF, Yu AC, Specks U, Ryu JH. Pulmonary involvement in Henoch-Schönlein purpura. Mayo Clin Proc 2004;79(9):1151–1157.

79. Sansonno D, Dammacco F. Hepatitis C virus, cryoglobulinaemia, and vasculitis: immune complex relations. Lancet Infect Dis 2005;5(4):227–236.

80. Ramos-Casals M, Robles A, Brito-Zerón P, et al. Life-threatening cryoglobulinemia: clinical and immunological characterization of 29 cases. Semin Arthritis Rheum 2006; 36(3):189–196.

81. Blanco R, Martínez-Taboada VM, Rodríguez-Valverde V, García-Fuentes M. Cutaneous vasculitis in children and adults: associated diseases and etiologic factors in 303 patients. Medicine (Baltimore) 1998;77(6): 403–418.

82. Koutkia P, Mylonakis E, Rounds S, Erickson A. Leucocytoclastic vasculitis: an update for the clinician. Scand J Rheumatol 2001;30(6):315–322.

83. Uzun O, Akpolat T, Erkan L. Pulmonary vasculitis in behcet disease: a cumulative analysis. Chest 2005;127(6):2243–2253.

84. Erkan F, Gül A, Tasali E. Pulmonary manifestations of Behçet's disease. Thorax 2001;56(7):572–578.

85. Hamuryudan V, Yurdakul S, Moral F, et al. Pulmonary arterial aneurysms in Behçet's syndrome: a report of 24 cases. Br J Rheumatol 1994;33(1):48–51.

86. Numan F, Islak C, Berkmen T, Tüzün H, Cokyüksel O. Behçet disease: pulmonary arterial involvement in 15 cases. Radiology 1994;192(2):465–468.

87. Tunaci M, Ozkorkmaz B, Tunaci A, Gül A, Engin G, Acuna B. CT findings of pulmonary artery aneurysms during treatment for Behcet's disease. AJR Am J Roentgenol 1999;172(3):729–733.

88. Slavin RE, de Groot WJ. Pathology of the lung in Behçet's disease: case report and review of the literature. Am J Surg Pathol 1981;5(8):779–788.

89. Chae EJ, Do KH, Seo JB, et al. Radiologic and clinical findings of Behçet disease: comprehensive review of multisystemic involvement. RadioGraphics 2008;28(5):e31.

90. Grenier P, Bletry O, Cornud F, Godeau P, Nahum H. Pulmonary involvement in Behcet disease. AJR Am J Roentgenol 1981; 137(3):565–569.

91. Lee J, Noh JW, Hwang JW, et al. Successful cyclophosphamide therapy with complete resolution of pulmonary artery aneurysm in Hughes-Stovin syndrome patient. Clin Rheumatol 2008;27(11):1455–1458.

92. Roberts DH, Jimenez JF, Golladay ES. Multiple pulmonary artery aneurysms and peripheral venous thromboses—the Hughes Stovin syndrome: report of a case in a 12-year-old boy and a review of the literature. Pediatr Radiol 1982;12(4):214–216.

93. Ketchum ES, Zamanian RT, Fleischmann D. Angiography of pulmonary artery aneurysms in Hughes-Stovin syndrome. AJR Am J Roentgenol 2005;185(2):330–332.

94. Reimold WV, Emmrich J, Harmjanz D, Kochsiek K. Multiple aneurysms of the pulmonary artery following recurrent septic pulmonary embolism (Hughes-Stovin syndrome): report of 1 case [in German]. Arch Klin Med 1968; 215(1):1–18.

95. Franks TJ, Koss MN. Pulmonary capillaritis. Curr Opin Pulm Med 2000;6(5):430–435.

96. Kim JS, Lee KS, Koh EM, Kim SY, Chung MP, Han J. Thoracic involvement of systemic lupus erythematosus: clinical, pathologic, and radiologic findings. J Comput Assist Tomogr 2000;24(1):9–18.

97. Zamora MR, Warner ML, Tuder R, Schwarz MI. Diffuse alveolar hemorrhage and systemic lupus erythematosus: clinical presentation, histology, survival, and outcome. Medicine (Baltimore) 1997;76(3):192–202.

98. Kim EA, Lee KS, Johkoh T, et al. Interstitial lung diseases associated with collagen vascular diseases: radiologic and histopathologic findings. RadioGraphics 2002;22(spec no):S151–S165.

99. Germain MJ, Davidman M. Pulmonary hemorrhage and acute renal failure in a patient with mixed connective tissue disease. Am J Kidney Dis 1984;3(6):420–424.

100. Sanchez-Guerrero J, Cesarman G, Alarcón-Segovia D. Massive pulmonary hemorrhage in mixed connective tissue diseases. J Rheumatol 1989;16(8):1132–1134.

101. Torralbo A, Herrero JA, Portolés J, Barrientos A. Alveolar hemorrhage associated with antineutrophil cytoplasmic antibodies in rheumatoid arthritis. Chest 1994; 105(5):1590–1592.

102. Haas C. Pulmonary hypertension associated with systemic lupus erythematosus. Bull Acad Natl Med 2004;188(6):985–997; discussion 997.

103. Pope J. An update in pulmonary hypertension in systemic lupus erythematosus: do we need to know about it? Lupus 2008;17(4):274–277.

104. Choi HK, Merkel PA, Walker AM, Niles JL. Drug-associated antineutrophil cytoplasmic antibody-positive vasculitis: prevalence among patients with high titers of antimyeloperoxidase antibodies. Arthritis Rheum 2000;43(2):405–413.

105. Dolman KM, Gans RO, Vervaat TJ, et al. Vasculitis and antineutrophil cytoplasmic autoantibodies associated with propylthiouracil therapy. Lancet 1993;342(8872):651–652.

106. Voorburg AM, van Beek FT, Slee PH, Seldenrijk CA, Schramel FM. Vasculitis due to gemcitabine. Lung Cancer 2002;36(2): 203–205.

107. Nicolls MR, Terada LS, Tuder RM, Prindiville SA, Schwarz MI. Diffuse alveolar hemorrhage with underlying pulmonary capillaritis in the retinoic acid syndrome. Am J Respir Crit Care Med 1998;158(4):1302–1305.

108. Han D, Lee KS, Franquet T, et al. Thrombotic and nonthrombotic pulmonary arterial embolism: spectrum of imaging findings. RadioGraphics 2003;23(6):1521–1539.

109. Kumar K, Holden WE. Drug-induced pulmonary vascular disease: mechanisms and clinical patterns. West J Med 1986;145(3): 343–349.

110. Lombard CM, Colby TV, Elliott CG. Surgical pathology of the lung in anti-basement membrane antibody-associated Goodpasture's syndrome. Hum Pathol 1989;20(5):445–451.

111. Anantham D, Chan KP, Chuah KL, Vathsala A, Eng P. Pulmonary capillaritis in IgA nephropathy. South Med J 2007;100(6):605–607.

112. Harland RW, Becker CG, Brandes JC, Fritsche C, Rosenzweig DY. Immunoglobulin A (IgA) immune complex pneumonitis in a patient with IgA nephropathy. Ann Intern Med 1992;116(3):220–222.